XAF1 inactivation increases tumor cell resistance to endoplasmic reticulum stress-induced apoptosis through stabilization of GRP78 and CHIP

Kyung-Woo Lee, Hui-Ra Hong, Ji-Sun Lim, Kyung-Phil Ko, Min-Goo Lee, and Sung-Gil Chi

Department of Life Sciences, Korea University, Seoul 02841, Republic of Korea

Running title: XAF1 promotes apoptotic ER stress response

Keywords: ER stress; XAF1; GRP78; ZNF313; CHIP

Correspondence: Sung-Gil Chi, Ph.D.

Department of Life Sciences, Korea University

Seoul 02841, Republic of Korea

Tel: +82-2-3290-3443

Fax: +82-2-927-5458

E-mail: chi6302@korea.ac.kr

SUMMARY

XAF1 expression is associated with apoptotic sensitivity of cells to ER stress.

XAF1 destabilizes GRP78 through the assembly of ZNF313-mediated destruction complex.

XAF1 blocks CHIP-IRE1α axis to drive apoptotic switch of UPR function.

Epigenetic inactivation of XAF1 enhances tumor cell resistance to ER stress.

Preprints (www.preprints.org) | NOT PEER-REVIEWED | Posted: 17 March 2022 doi:10.20944/preprints202203.0251.v1

ABSTRACT

Despite accumulating evidence for the pro-apoptotic role for X-linked inhibitor of apoptosis-associated factor 1 (XAF1), its involvement in endoplasmic reticulum (ER) stress response remains undefined. Here, we report that XAF1 enhances cell sensitivity to ER stress and acts as a switch in unfolded protein response (UPR)-mediated cell-fate decisions favoring apoptosis over adaptive autophagy. XAF1 interacts with and destabilizes ER stress sensor GRP78 through the assembly of zinc finger protein 313-mediated destruction complex. Moreover, *XAF1* gene transcription is activated by ER stress through PERK-Nrf2 signaling to direct an adaptive to apoptotic switch of stress response by blocking C-terminus of Hsc70-interacting protein (CHIP)-mediated K63-linked ubiquitination and subsequent phosphorylation of inositol-required enzyme-1α (IRE1α). In tumor xenograft assays, *XAF1*$^{-/-}$ tumors display substantially lower regression compared to *XAF1*$^{+/+}$ tumors in response to cytotoxic dose of ER stress inducer. XAF1 and GRP78 expression show an inverse correlation in human cancer cell lines and primary breast carcinomas. Collectively this study uncovers an important role for XAF1 as a linchpin to govern the sensitivity to ER stress and the outcomes of UPR signaling, illuminating the mechanistic consequence of *XAF1* inactivation in tumorigenesis.

Preprints (www.preprints.org) | NOT PEER-REVIEWED | Posted: 17 March 2022 doi:10.20944/preprints202203.0251.v1

INTRODUCTION

Endoplasmic reticulum (ER) is a central organelle responsible for the synthesis, maturation, and transportation of proteins [1, 2]. Perturbation of ER homeostasis causes the accumulation of excessive unfolded or misfolded proteins, which is referred to as ER stress [3]. ER stress is sensed by a quality control mechanism termed unfolded protein response (UPR), which aims to maintain the proteostasis in the ER lumen by increasing protein folding capacity and misfolded protein degradation [4, 5].

Glucose-regulated protein (GRP78), also called BiP or HSPA5, is a major ER chaperone protein that acts as an ER stress sensor [3]. GRP78 is primarily located in the ER but also detected in the cell surface, cytosol, and mitochondria [6]. In unstressed cells, GRP78 binds to three transmembrane UPR transducers, inositol-required enzyme-1 (IRE1), protein kinase RNA-like endoplasmic reticulum kinase (PERK) and activating transcription factor 6 (ATF6) to keep them in an inactive state. In response to ER stress, GRP78 is redirected from these UPR proteins to misfolded proteins and UPR signaling is initiated to facilitate the proteasomal degradation of misfolded proteins [7, 8]. The maintenance of ER integrity and proteostasis is essential for rapidly growing cancer cells [9, 10]. Expression of GRP78 is associated with ER integrity and enhanced cell survival [11, 12]. High expression of GRP78 is observed in multiple human cancers and correlates with malignant progression and tumor resistance to etoposide, cisplatin, temozolomide, and γ-radiation [4, 13-16].

X-linked inhibitor of apoptosis (XIAP)-associated factor 1 (XAF1) is a pro-apoptotic tumor suppressor that is originally found to antagonize the anti-caspase activity of XIAP [17]. Epigenetic inactivation of *XAF1* due to aberrant promoter hypermethylation is observed in a broad range of human cancers and associates with the stage and grade of many tumors [18-21]. The *XAF1* gene encodes 33 kDa protein that contains seven zinc finger (ZF) domains, suggesting its role in the regulation of protein-protein interaction [17]. XAF1 interacts with many proteins, including zinc

Preprints (www.preprints.org) | NOT PEER-REVIEWED | Posted: 17 March 2022 doi:10.20944/preprints202203.0251.v1

finger protein 313 (ZNF313) ubiquitin E3 ligase and homeodomain-interacting protein kinase 2 and can promote apoptosis through multiple XIAP-independent mechanisms [22-24].

XAF1 transcription is activated in response to various genotoxic, oxidative, and cytokine stresses to drive apoptosis induction [20, 21]. In particular, *XAF1* is strongly activated by interferons and sensitizes cells to the pro-apoptotic actions of interferons and tumor necrosis factor -related apoptosis inducing ligand [23-25]. XAF1 also regulates autophagy, tumor angiogenesis, and G2/M checkpoint of the cell cycle [27, 28]. Our studies show that XAF1 is activated by the p53 tumor suppressor and acts as a molecular switch in p53-mediated cell-fate decisions favoring apoptosis over cell-cycle arrest [23]. XAF1 forms a feedback loop with interferon regulatory factor-1 (IRF-1) and evokes its tumor suppression effect in a highly IRF-1-dependent fashion [29]. Recently, we reported that XAF1 is activated by heavy metals and triggers an apoptotic conversion of stress response by binding and destabilizing metallothionein 2A [30].

Despite accumulating evidence for the apoptosis-promoting role for XAF1 under various stressful conditions, its role in ER stress response remains undefined. In the present study, we found that XAF1 enhances cell sensitivity to ER stress through GRP78 destabilization and its induction drives an apoptotic switch of UPR function by blocking IRE1α phosphorylation. Therefore, this study uncovers an important role for XAF1 in UPR-mediated cell-fate decisions.

RESULTS

XAF1 expression enhances apoptotic response to ER stress

To explore the role for XAF1 in ER stress response, we initially tested whether its expression influences apoptotic response to ER stress using 24 human cancer cell lines. A flow cytometric measurement of apoptotic sub-G1 fraction revealed that XAF1 expression level is associated with apoptotic sensitivity to the ER stress inducer thapsigargin (TG) (Fig. 1A, B). Based on this, we examined effect of gene knockout and stable overexpression of XAF1 using J82 and T47D cell

Preprints (www.preprints.org) | NOT PEER-REVIEWED | Posted: 17 March 2022 doi:10.20944/preprints202203.0251.v1

lines, respectively. Compared to J82-*XAF1*$^{+/+}$ subline, J82-*XAF1*$^{-/-}$ subline showed markedly reduced apoptotic response to TG and other ER stress inducers, tunicamycin (TM) and brefeldin A (BFA) (Fig. 1C-E). A rescue experiment showed that J82-*XAF1*$^{-/-}$ cells recover the apoptotic sensitivity to TG if XAF1 expression is restored (Supplementary Fig. 1A). Consistently, T47D-XAF1 subline exhibited increased sensitivity to the ER stress inducers compared to T47D-pcDNA subline (Fig. 1D, F). A series of assays using transient knockdown and overexpression or tetracycline-inducible XAF1 (Tet-XAF1) system confirmed that XAF1 enhances tumor cell sensitivity to ER stress-induced apoptosis (Supplementary Fig. 1B-E).

Autophagy is a representative adaptive response to ER stress [32]. However, autophagy also can lead to cell death, indicating that autophagy pathway can be subverted from a survival to a death function [33]. We asked whether XAF1 promotes apoptosis through the regulation of autophagy. Compared to J82-*XAF1*$^{-/-}$ and T47D-pcDNA sublines, J82-*XAF1*$^{+/+}$ and T47D-XAF1 sublines displayed higher autophagic response (increased LC3-I/II) (Fig. 1G, H). Immunoblot (IB) assays of autophagy markers, such as Beclin-1, and Atg5-Atg12, in LoVo sublines (*XAF1*$^{+/+}$ and *XAF1*$^{-/-}$) and T47D (Tet-XAF1) cells also showed that XAF1 induction of apoptosis is associated with its stimulation of autophagy (Supplementary Fig. 1F-H). As predicted, blockade of autophagy by 3-MA treatment caused apoptosis reduction in J82-*XAF1*$^{+/+}$ and T47D-XAF1 cells (Fig. 1G-I). By contrast, in J82-*XAF1*$^{-/-}$ and T47D-pcDNA cells, 3-MA treatment resulted in apoptosis induction. This observation supports that autophagy exerts protective role in XAF1-nonexpressing cells and that XAF1 expression facilitates autophagy to drive ER stress-mediated apoptosis. Consistently, immunofluorescence (IF) assay of LC3B puncta revealed that XAF1 increases TG-induced LC3B puncta and this effect is abrogated by 3-MA (Fig. 1J and Supplementary Fig. 1I). To define whether XAF1 induction of LC3B puncta results from autophagy activation or its lysosomal accumulation due to inhibition of autophagic flux, effects of 3-MA (inhibitor of early autophagy) and BafA1 (inhibitor of late autophagy) were compared. XAF1 induction of LC3B puncta was blocked by

Preprints (www.preprints.org) | NOT PEER-REVIEWED | Posted: 17 March 2022 doi:10.20944/preprints202203.0251.v1

3-MA but increased by BafA1, indicating that XAF1 facilitates autophagic flux (Fig. 1J, Supplementary Fig. 1I). Together, these support that XAF1 stimulates autophagy-mediated apoptosis under ER stress conditions.

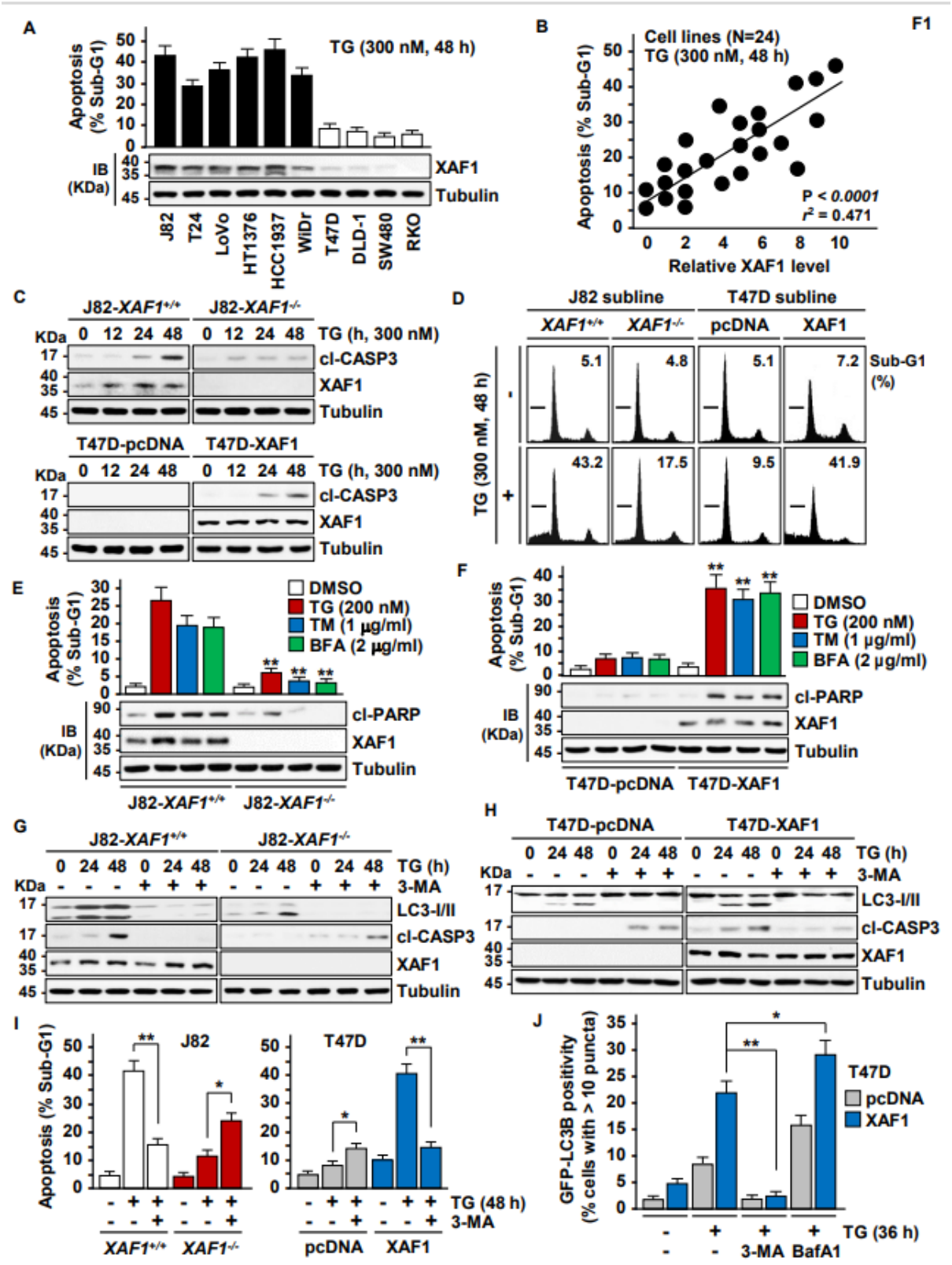

Preprints (www.preprints.org) | NOT PEER-REVIEWED | Posted: 17 March 2022 doi:10.20944/preprints202203.0251.v1

Fig. 1 XAF1 expression is associated with cytotoxic ER stress response. A, B XAF1 expression and its association with apoptotic tumor cell response to TG. Apoptosis was determined by flow cytometric measurement of sub-G1 fraction. IB, immunoblot. r^2, Pearson's correlation coefficient. **C-F** Effect of XAF1 knockout and stable overexpression on ER stress-induced apoptosis. J82 and T47D sublines were treated with TG, TM, and BFA as indicated. IB assay of cleaved caspase-3 (cl-CASP3) and flow cytometric assay of sub-G1 fraction were performed to detect apoptosis induction. **G-I** XAF1 stimulation of TG-induced autophagy and effect of its inhibition on apoptosis induction. J82 and T47D sublines were exposed to 3-MA (5 μM) at 2 h before TG treatment (200 nM). **J** Immunofluorescence microscopic analysis of LC3B puncta showing autophagy-stimulating function of XAF1. GFP-LC3 and RFP-XAF1 were transfected to detect LC3B puncta and XAF1 expression, respectively. Cells were exposed to 3-MA (5 μM) or BafA1 (100 nM) at 2 h before TG treatment (200 nM). Data represent the mean ± SD of triplicate assays. * $P < 0.05$; ** $P < 0.01$ (Student *t* test).

XAF1 activates ER stress-induced UPR signaling through GRP78 destabilization

We examined XAF1 effect on ER stress-mediated UPR signaling. In response to TG treatment, J82-*XAF1*$^{+/+}$ cells showed higher activation of UPR transducers (PERK, IRE1α, and ATF6) and their downstream effectors (CHOP, XBP1s, elF2α, and ATF4) compared to J82-*XAF1*$^{-/-}$ cells (Fig. 2A). Consistently, TG activation of UPR signaling was reinforced by XAF1 overexpression in T47D cells while it was attenuated by XAF1 depletion in LoVo cells (Supplementary Fig. 2A, B). Based on this observation, we tested whether XAF1 regulates GRP78, a chaperone protein acting as a master switch of UPR signaling [7, 8]. GRP78 protein but not mRNA expression was markedly increased and decreased by XAF1 depletion and expression, respectively (Fig. 2B and Supplementary Fig. 2C-F). J82-*XAF1*$^{-/-}$ cells showed a much higher GRP78 level compared to J82-*XAF1*$^{+/+}$ cells and XAF1 restoration decreased GRP78 level in J82-*XAF1*$^{-/-}$ cells (Fig. 2C, D). XAF1 stabilizes or destabilizes multiple proteins through interaction with ubiquitin E3 ligases [22, 23, 34]. We assessed XAF1 effect on the protein stability of GRP78. A cycloheximide (CHX) assay revealed that XAF1 induction shortens the half-life of GRP78 protein from approximately 4.3 h to 2.4 h (Fig. 2E, F). XAF1-mediated GRP78 degradation was completely blocked by the proteasome inhibitor MG132, but not affected by the lysosome inhibitor leupeptin, indicating that XAF1

Preprints (www.preprints.org) | NOT PEER-REVIEWED | Posted: 17 March 2022 doi:10.20944/preprints202203.0251.v1

destabilizes GRP78 through the proteasomal pathway (Fig. 2G). Immunoprecipitation (IP) assay showed that XAF1 increases ubiquitination of GRP78 (Fig. 2H). Additionally, a strong inverse correlation was identified between XAF1 and GRP78 levels in 21 human cancer cell lines (Fig. 2I, J). To ascertain the clinical relevance of XAF1-GRP78 relationship, we analyzed their expression status in human breast tissues. Immunohistochemistry (IHC) study of 70 primary breast tumor tissues revealed a frequent reduction of XAF1 in tumor versus normal tissues and its inverse correlation with GRP78 expression (Fig. 2K, L).

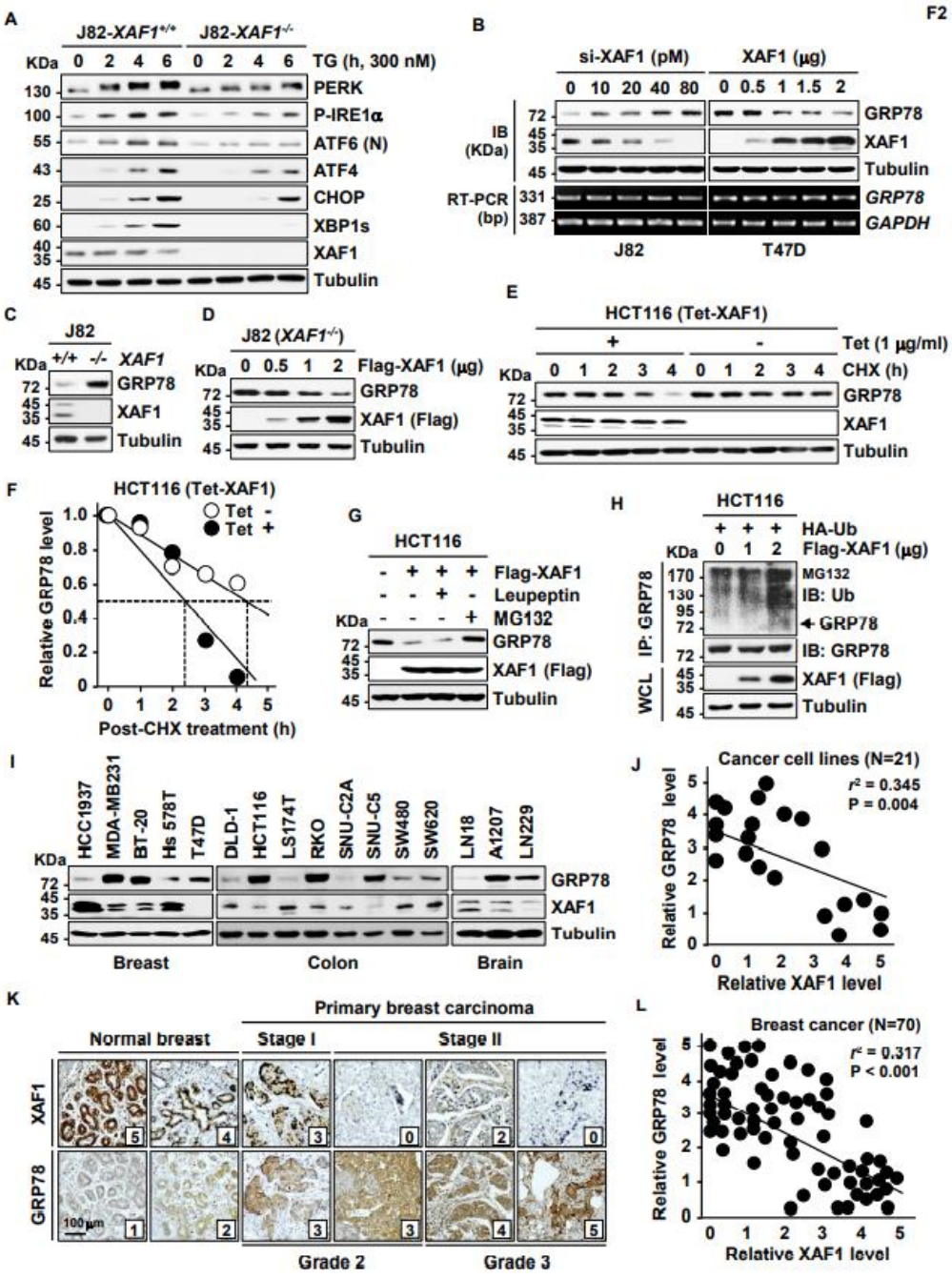

Preprints (www.preprints.org) | NOT PEER-REVIEWED | Posted: 17 March 2022 doi:10.20944/preprints202203.0251.v1

Fig. 2 XAF1 induces GRP78 degradation to activate UPR signaling. A Comparison of *XAF1*$^{+/+}$ and *XAF1*$^{-/-}$ sublines of J82 in TG-induced UPR signaling. **B** Effect of XAF1 depletion and expression on GRP78 expression. Cells were transfected with increasing doses of si-XAF1 or XAF1. GRP78 protein and mRNA levels were examined at 48 h after transfection. **C** Comparison of GRP78 protein level in J82-*XAF1*$^{+/+}$ and J82-*XAF1*$^{-/-}$ sublines. **D** Effect of XAF1 restoration on GRP78 expression in J82-*XAF1*$^{-/-}$ cells. **E, F** A CHX chase experiment showing GRP78-destabilizing effect of XAF1. Cells were exposed to CHX (40 μM) for indicated times. XAF1 expression was achieved using Tet-inducible XAF1 system (Tet-XAF1). **G** Impairment of XAF1-mediated GRP78 reduction by MG132. Cells transfected with Flag-XAF1 were exposed to MG132 (10 μM) or Leupeptin (10 μM) for 6 h. **H** IP assay showing XAF1 induction of GRP78 ubiquitination. HA, hemagglutinin; Ub, ubiquitin; WCL, whole cell lysate. **I, J** An inverse correlation of XAF1 and GRP78 protein levels in human cancer cell lines. r^2, Pearson's correlation coefficient. **K, L** IHC assay of XAF1 and GRP78 expression (dark brown) in human breast carcinoma and normal tissues. Relative staining levels were classified as levels 0-5. r^2, Pearson's correlation coefficient.

XAF1 promotes GRP78 degradation through direct interaction

To further address the mechanism underlying XAF1-induced GRP78 destabilization, we examined whether XAF1 binds to GRP78. IP and *in vitro* GST pull-down assays revealed that XAF1 binds to GRP78 (Fig. 3A-C). IF assay of GRP78 and XAF1 cellular localization supported their interaction (Supplementary Fig.3A). Using a series of deletion mutants, we identified that the C-terminal region including zinc finger 7 (ZF7) domain of XAF1 is responsible for the interaction (Fig. 3D-F). Unlike wild-type (WT) XAF1, a mutant XAF1 lacking the GRP78-interacting region (Δ7C-XAF1) showed no activity to induce ubiquitination and reduction of GRP78 (Fig. 3G, H). As predicted, Δ7C-XAF1 failed to promote TG-induced apoptosis (Fig. 3I, J). These indicate that XAF1 enhances apoptotic ER stress response through interaction-mediated destabilization of GRP78.

Preprints (www.preprints.org) | NOT PEER-REVIEWED | Posted: 17 March 2022 doi:10.20944/preprints202203.0251.v1

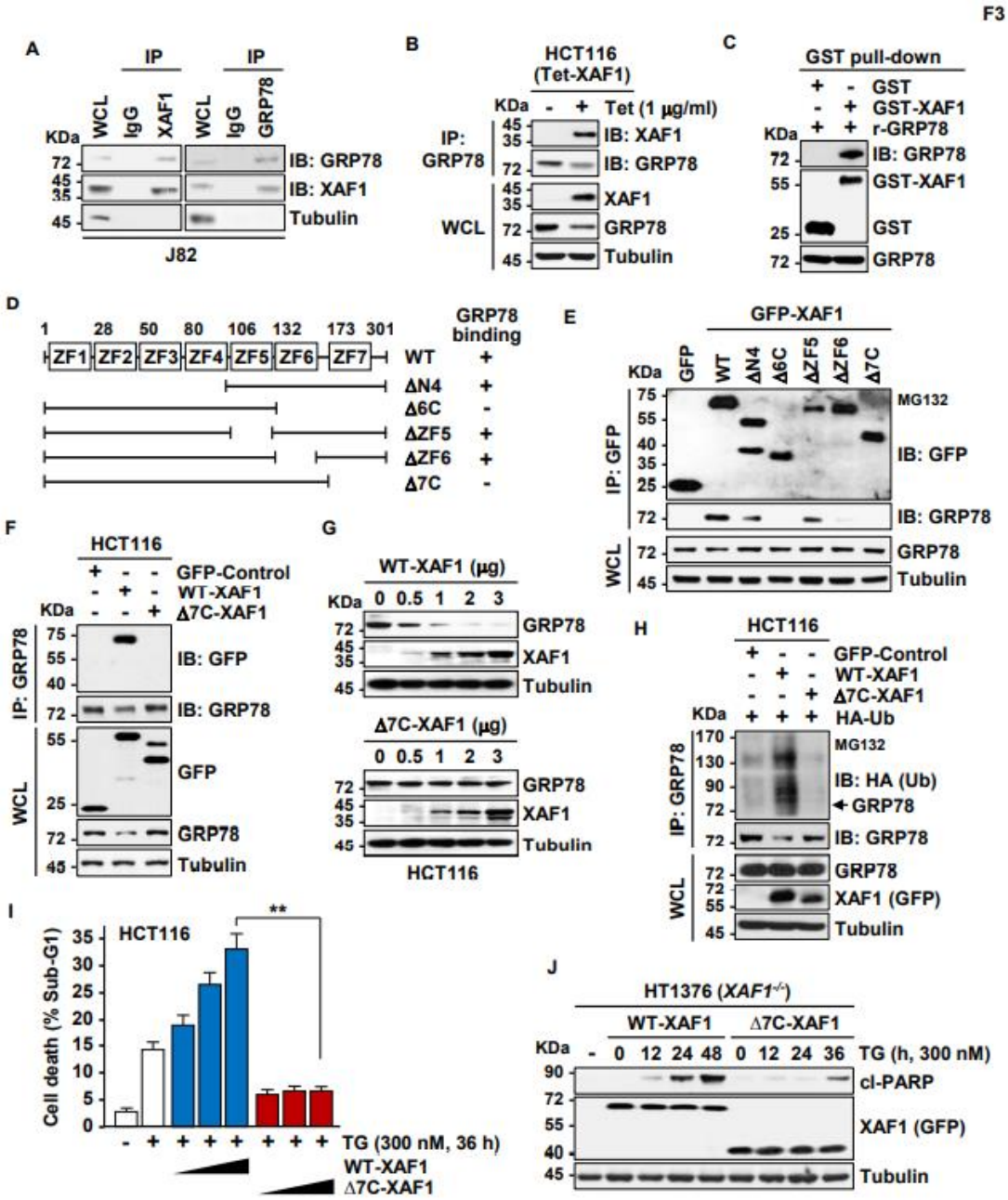

Fig. 3 XAF1 binds directly to GRP78. A, B IP assays showing XAF1 interaction with GRP78. **C** *In vitro* GST pull-down assay showing the direct interaction of purified GST-XAF1 and recombinant GRP78 proteins. GST, glutathionine S-transferase; r, Recombinant. **D** Deletion mutants of XAF1 and their GRP78-binding status. ZF, zinc finger; WT, wild-type. **E-G** IP assays showing a critical role for ZF7-containing C-terminal region (7C) of XAF1 in binding and downregulation of GRP78. **H** No GRP78 ubiquitination-inducing ability of Δ7C-XAF1. **I, J** No apoptosis-promoting activity of Δ7C-XAF1. Cells were transfected with either WT-XAF1 or Δ7C-XAF1 and then treated with TG (300 nM). Apoptosis induction was determined by flow cytometric analysis of sub-G1 fraction and IB assay of cleaved PARP level. Data represent the mean ± SD of triplicate assays. ** $P < 0.01$ (Student *t* test).

Preprints (www.preprints.org) | NOT PEER-REVIEWED | Posted: 17 March 2022 doi:10.20944/preprints202203.0251.v1

XAF1 destabilizes GRP78 through the assembly of ZNF313-mediated destruction complex

To identify an E3 ligase responsible for XAF1-induced GRP78 ubiquitination, we tested the involvement of ZNF313, which is known to interact with XAF1 [22]. XAF1-induced GRP78 reduction was totally impaired in ZNF313-depleted cells while GRP78 level was markedly decreased by ectopic overexpression of ZNF313 (Fig. 4A, Supplementary Fig. 4A). Moreover, ZNF313 overexpression strongly increased ubiquitination of GRP78 (Supplementary Fig. 4B). A series of interaction assays revealed that ZNF313 binds directly to GRP78 through the N-terminus including the RING domain (Fig. 4B, C, Supplementary Fig. 4C). Unlike WT-ZNF313, a RING mutant (RING-MT), which has C-to-G sequence replacement at codons 29 and 32 in the RING domain, failed to interact with GRP78 and showed no activity to increase GRP78 ubiquitination (Fig. 4D-F). Furthermore, IP assay showed that ZNF313-GRP78 interaction is reinforced in a XAF1 transfection dose-associated manner (Fig. 4G). TG treatment increased ZNF313-GRP78 interaction in *XAF1*$^{+/+}$ but not in *XAF1*$^{-/-}$ subline of HT1376 cells (Fig. 4H). XAF1-induced ubiquitination and downregulation of GRP78 was clearly seen in *ZNF313*$^{+}$ but not in *ZNF313*$^{-}$ subline of the HAP1 haploid human cell line, further supporting the ZNF313-dependency of XAF1 regulation of GRP78 (Fig. 4I). As predicted, XAF1's function to promote TG-induced apoptosis was impeded in ZNF313-depleted cells (Fig. 4J). These indicate that XAF1 stimulates GRP78 degradation by enhancing ZNF313 interaction with and ubiquitination of GRP78.

Preprints (www.preprints.org) | NOT PEER-REVIEWED | Posted: 17 March 2022 doi:10.20944/preprints202203.0251.v1

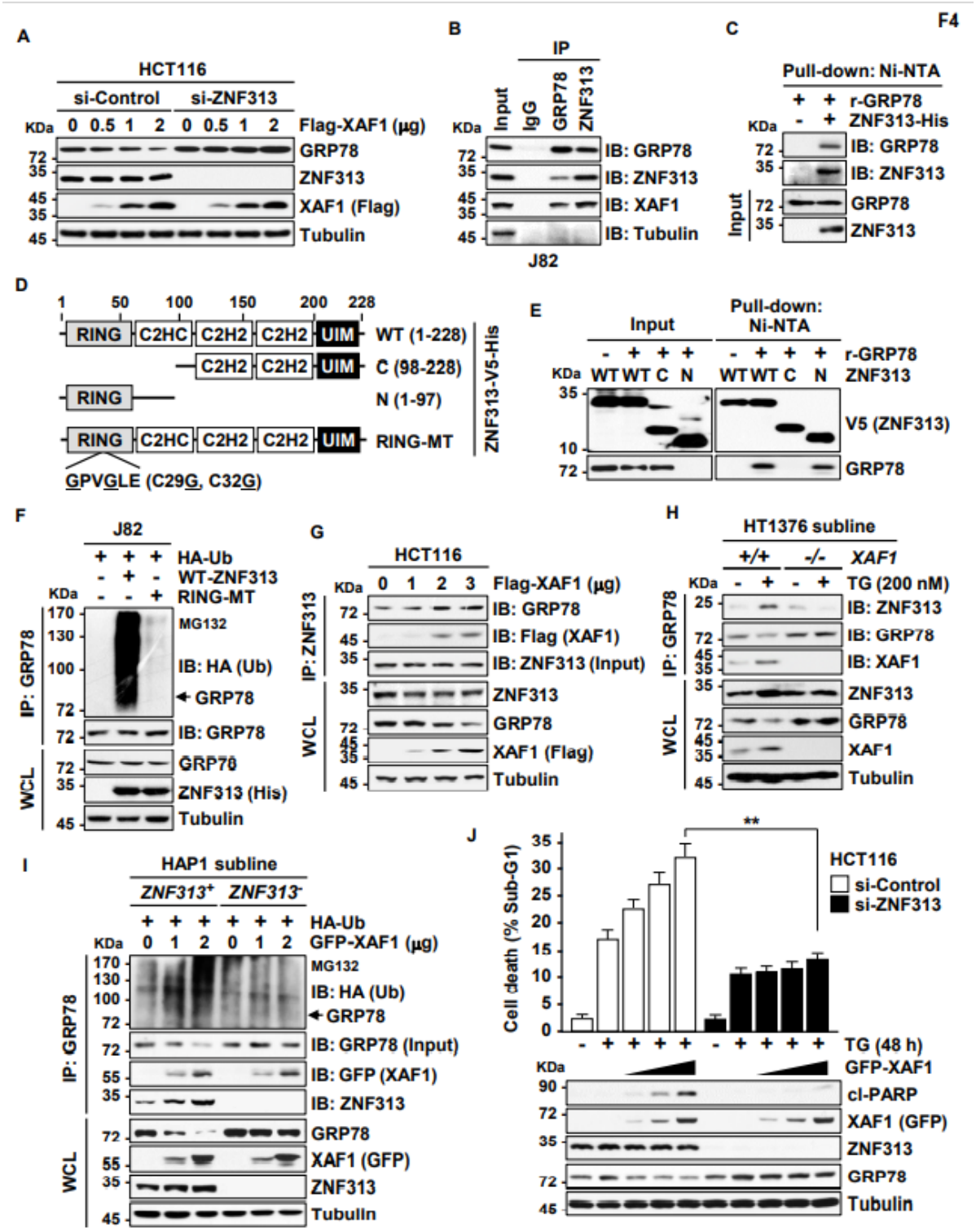

Fig. 4 XAF1 promotes ZNF313-GRP78 interaction to facilitate GRP78 ubiquitination. A Effect of ZNF313 depletion on XAF1-mediated GRP78 reduction. Cells were transfected with 50 pM of si-Control or si-ZNF313 and IB assay was carried out at 48 h after transfection. **B** IP assay showing XAF1 interaction with GRP78. **C** *In vitro* GST pull-down assay showing the direct interaction of purified ZNF313-His and recombinant GRP78 (r-GRP78). **D** Construction of deletion mutants of ZNF313 for characterization of GRP78-interacting region. RING, Really Interesting New Gene; UIM, ubiquitin-interacting motif; MT, mutant. **E,** A Ni-NTA pull-down

Preprints (www.preprints.org) | NOT PEER-REVIEWED | Posted: 17 March 2022 doi:10.20944/preprints202203.0251.v1

assay for the GRP78-interacting activity of WT and deletion mutants of ZNF313. **F** Loss of GRP78-ubiquitinating activity by RING mutation. **G** XAF1 stimulation of ZNF313-GRP78 interaction. IP was performed using equal amount of ZNF313 input. **H** Effect of *XAF1* knockout on TG-induced ZNF313-GRP78 interaction. **I** Validation of a ZNF313 dependency of XAF1 stimulation of ZNF313-GRP78 interaction and GRP78 ubiquitination. XAF1 effect was compared in HAP1 *ZNF313*$^{+}$ and *ZNF313*$^{-}$ subline cells. **J** Effect of ZNF313 depletion on XAF1 stimulation of TG-induced apoptosis. Data represent the mean ± SD of triplicate assays. ** $P < 0.01$ (Student *t* test).

XAF1 transcription is activated by ER stress through PERK-Nrf2 signaling

Our results have shown that the methylation status of the *XAF1* promoter is associated with apoptotic response to ER stress (Fig. 1A, B). We also recognized that apoptotic response to ER stress is strongly associated with XAF1 induction, suggesting that XAF1 activation may direct an apoptotic switch of UPR function while its basal expression enhances the sensitivity to ER stress through GRP78 destabilization (Fig. 5A, B, Supplementary Fig. 5A). To address this issue, we characterized signaling pathway that is responsible for the ER stress-mediated XAF1 induction. ER stress activates transcription of multiple genes mainly through UPR signaling [3]. We thus asked whether XAF1 induction occurs through UPR signaling. *XAF1* mRNA expression was upregulated by TG, TM, and BFA and this induction was abrogated by pretreatment of actinomycin D (Act D), an inhibitor of *de novo* RNA synthesis, indicating the transcriptional activation of *XAF1* by ER stress (Supplementary Fig. 5B, C). Moreover, assays using increasing exposure times and doses revealed that XAF1 induction is tightly linked to apoptotic response to TG, suggesting that XAF1 induction may act as a switch in cell-fate decisions under ER stress conditions (Fig. 5C, D, Supplementary Fig. 5D, E). *XAF1* induction by TG was strongly impeded by depletion of PERK or its inhibitor GSK2606414 but not affected by depletion of IRE1α or ATF6 (Fig. 5E, Supplementary Fig. 5F, G). It was also blocked by depletion of a PERK effector nuclear factor erythroid 2-related factor 2 (Nrf2) but not affected by another effector ATF4, indicating that *XAF1* transcription is activated through PERK-Nrf2 signaling (Fig. 5F, Supplementary Fig. 5H). Consistently, *XAF1* mRNA was induced by PERK overexpression and PERK activation of XAF1

Preprints (www.preprints.org) | NOT PEER-REVIEWED | Posted: 17 March 2022 doi:10.20944/preprints202203.0251.v1

was abolished by Nrf2 (Supplementary Fig. 5I). We identified a putative Nrf2 response element (ARE) in the 5′ upstream region (nucleotides -1055 to -1084 relative to ATG) of the *XAF1* gene (Fig. 5G). The activity of reporters containing this ARE (Pro1537 and Pro1123) was strongly activated by TG treatment while a reporter omitting the ARE (Pro1055) showed no response to TG (Fig. 5H). The Pro1123 reporter response to TG was significantly decreased by depletion of either PERK or Nrf2 but not affected by depletion of IRE1α or ATF6 (Fig. 5I, Supplementary Fig. 5J). A chromatin immunoprecipitation (ChIP) assay showed that the ARE within the *XAF1* promoter is occupied directly by Nrf2 (Fig. 5J). These indicate that *XAF1* is a *bona fide* transcription target of Nrf2 whose activation drives apoptotic ER stress response.

Fig. 5 *XAF1* transcription is activated by ER stress via PERK-Nrf2 signaling. A XAF1 upregulation by TG and its association with apoptosis induction in human cell lines. **B** Immunofluorescence microscopic analysis of XAF1 in HCC1937 cells. Cells were treated with DMSO (control) or TG (300 nM) for 24 h. DAPI was used for counterstaining of the nuclei. **C** A time kinetics of *XAF1* mRNA induction following TG exposure and its association with apoptosis induction. **D** Activation of *XAF1* mRNA expression by cytotoxic doses of TG. **E, F** Disruption of TG induction of *XAF1* mRNA by depletion of PERK or Nrf2. Cells were transfected with 50 pM of si-RNAs as indicated and then exposed to TG (300 nM) for 12 h. **G** A putative ARE in the *XAF1* promoter and reporter construction for luciferase assay. Luc, luciferase. **H, I** TG activation of the reporter containing the putative ARE and its attenuation by depletion of PERK or Nrf2. Cells were transfected with the reporters and then exposed to TG (300 nM) for 12 h. **I** ChIP assays showing Nrf2 binding to the ARE in TG-treated cells. Cells were exposed to TG (300 nM) for 12 h. α-Nrf2, Nrf2-specific antibody. Data represent the mean ± SD of triplicate assays. ** $P < 0.01$ (Student *t* test).

Preprints (www.preprints.org) | NOT PEER-REVIEWED | Posted: 17 March 2022 doi:10.20944/preprints202203.0251.v1

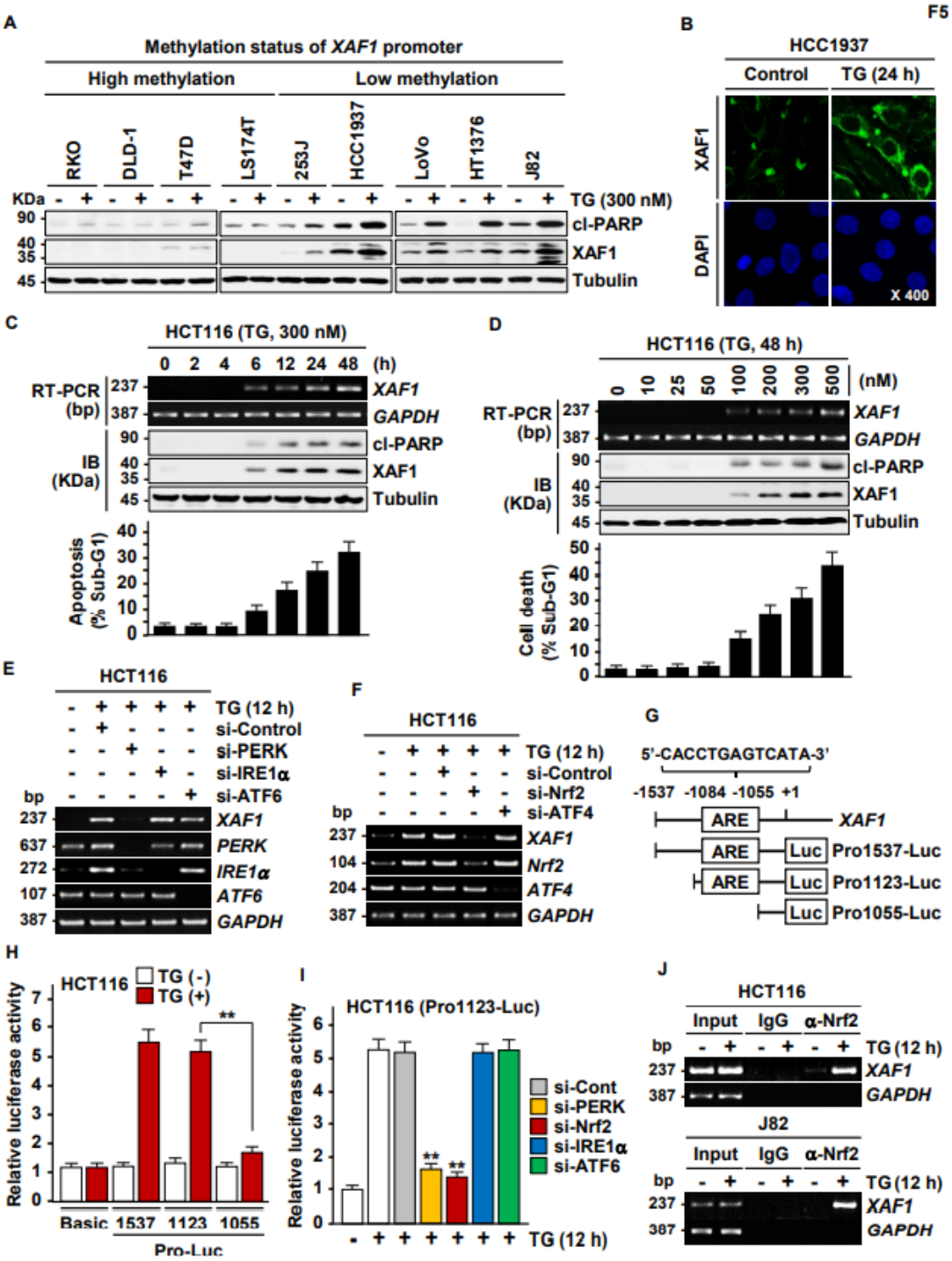

XAF1 blocks CHIP-IRE1α axis to direct apoptotic switch of ER stress response

ER stress response is determined mainly by UPR signaling pathways [3]. We assessed whether XAF1 drives ER stress-mediated apoptosis through the regulation of UPR signalings. Following TG treatment, IRE1α displayed much higher and prolonged phosphorylation in J82-*XAF1*$^{-/-}$

Preprints (www.preprints.org) | NOT PEER-REVIEWED | Posted: 17 March 2022 doi:10.20944/preprints202203.0251.v1

compared to J82-*XAF1*$^{+/+}$ subline while PERK and ATF6 showed comparable activation kinetics in both sublines (Fig. 6A). IRE1 activity was reported to attenuate under irresolvable ER stress to induce apoptosis [35, 36]. In J82-*XAF1*$^{+/+}$ cells, XAF1 induction was apparent at 6 h after TG treatment and associated with a decline of IRE1α phosphorylation and induction of apoptosis. TG-mediated IRE1α phosphorylation and expression of its effector XBP1s were further reinforced by XAF1 depletion in a si-XAF1 dose-associated manner, supporting that XAF1 represses the IRE1α signaling pathway (Supplementary Fig. 6A). To further define effect of XAF1 induction, we utilized *XAF1*$^{-/-}$ sublines (HT1376 and T47D) with the Tet-inducible XAF1 system and co-treatment of TG and Tet. In both cells, a clear decline of TG-induced IRE1α phosphorylation and XBP1s expression was detected from 6 h post-treatment at which XAF1 was induced (Fig. 6B, C). The E3 ligase C-terminus of Hsc70-interacting protein (CHIP) increases IRE1α phosphorylation through K63-linked ubiquitination, which is associated with adaptive response to ER stress and cell survival [37]. Consistently, we observed that TG induction of IRE1α phosphorylation is substantially attenuated in CHIP-depleted cells (Supplementary Fig. 6B). Recently, we reported that XAF1 decreases CHIP expression [29]. On this basis, we asked whether XAF1 suppression of IRE1α phosphorylation occurs through CHIP downregulation. Transient transfection or Tet-mediated induction of XAF1 led to a drastic decrease in CHIP protein level and its effects on TG-induced IRE1α phosphorylation and apoptosis were profoundly impeded in CHIP-depleted cells (Fig. 6D, E, Supplementary Fig. 6C-E). As predicted, the half-life of CHIP protein was substantially shortened by XAF1 induction and this effect was blocked by MG132, indicating that XAF1 induces the proteasomal degradation of CHIP (Fig. 6F, Supplementary Fig. 6F). Finally, we tested if XAF1 inhibits CHIP-mediated K63-linked ubiquitination of IRE1α. IP assay revealed that XAF1 suppresses K63-linked ubiquitination of IRE1α induced by TG treatment or CHIP transfection and this effect of XAF1 was accompanied with CHIP reduction (Fig. 6G, H,

Preprints (www.preprints.org) | NOT PEER-REVIEWED | Posted: 17 March 2022 doi:10.20944/preprints202203.0251.v1

Supplementary Fig. 6G). These indicate that XAF1 induction directs an apoptotic switch of ER stress response by blocking the adaptive CHIP-IRE1α axis.

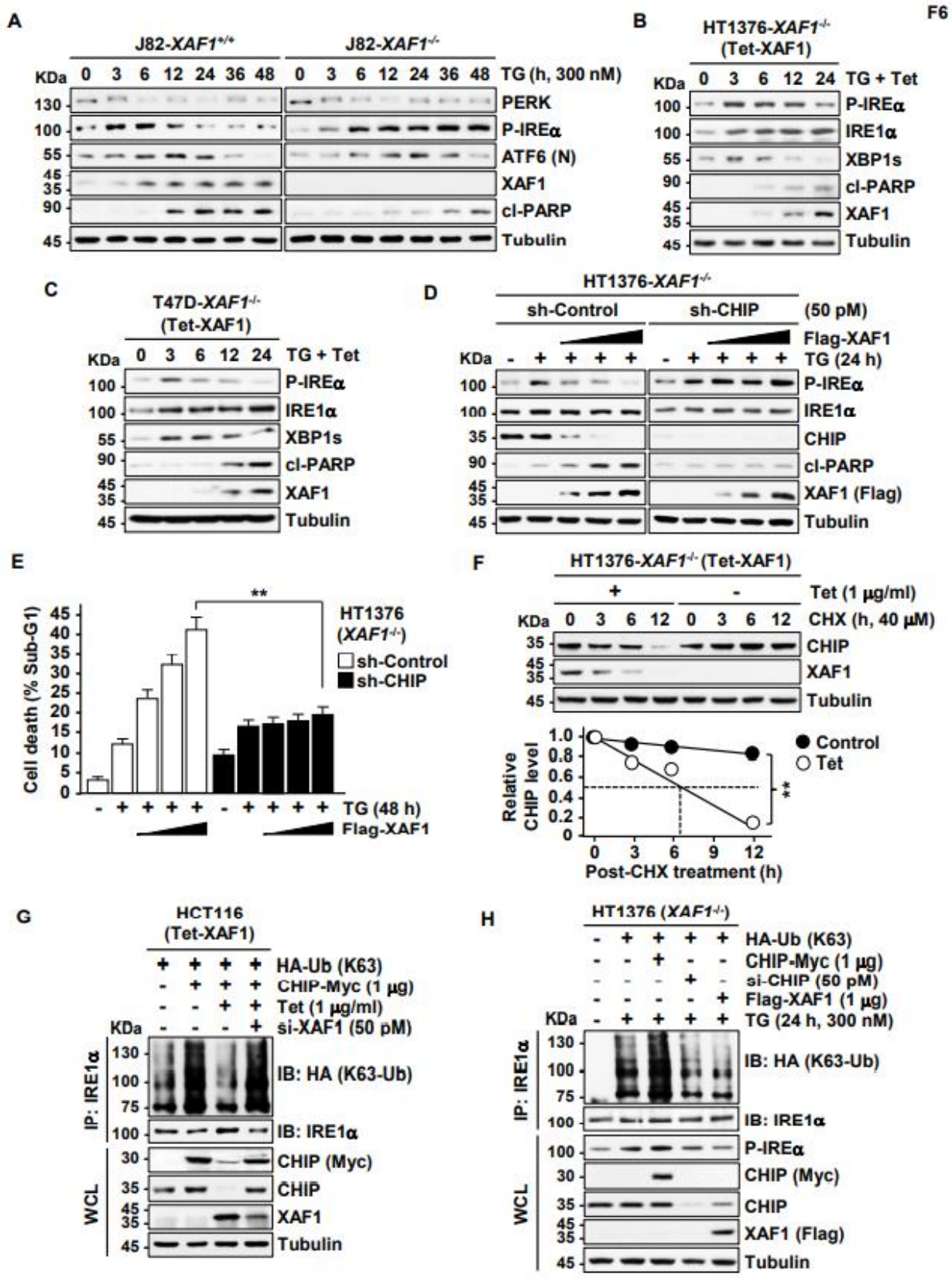

Preprints (www.preprints.org) | NOT PEER-REVIEWED | Posted: 17 March 2022 doi:10.20944/preprints202203.0251.v1

Fig. 6 XAF1 inhibits IRE1α phosphorylation by destabilizing CHIP. A Comparison of TG activation of three UPR transducers in *XAF1*$^{+/+}$ and *XAF1*$^{-/-}$ sublines of J82 cells. **B, C** Effect of XAF1 expression on TG-induced IRE1α phosphorylation and XBP1s expression in *XAF1*$^{-/-}$ cells. Cells were treated with TG (300 nM) and XAF1 induction was achieved by Tet-inducible XAF1 (Tet-XAF1) system. **D, E** A CHIP dependency of XAF1 effect on TG-induced IREα phosphorylation and apoptosis. Cells were treated with TG (300 nM). **F** CHX chase experiment showing XAF1 destabilization of CHIP. XAF1 induction was achieved by Tet-inducible XAF1 (Tet-XAF1) system. Cells were incubated with CHX (40 μM) for indicated hours. **G, H** Effect of XAF1 expression on CHIP or TG-induced K63-linked ubiquitination of IREα.

XAF1 enhances therapeutic effect of ER stress inducer *in vivo*

To investigate the XAF1 role in tumor response to TG *in vivo*, we carried out mouse tumor xenograft assays using *XAF1*$^{+/+}$ and *XAF1*$^{-/-}$ sublines of LoVo cells. Compared to *XAF1*$^{+/+}$ tumors, *XAF1*$^{-/-}$ tumors displayed an increased growth rate (Fig. 7A, B). In response to a cytotoxic dose of TG (12 μg/kg), *XAF1*$^{-/-}$ tumors showed much lower regression compared to *XAF1*$^{+/+}$ tumors (16.7% versus 78.6%). IB assay of xenograft tissues revealed that *XAF1*$^{-/-}$ tumors have higher GRP78, CHIP, and phosphorylated IRE1α levels compared to *XAF1*$^{+/+}$ tumors (Fig. 7C). Collectively, our study identifies XAF1 as a key regulator of ER stress response, illuminating its novel role as a tumor suppressor and the mechanistic consequence of its epigenetic alteration in tumorigenesis (Fig. 7D).

Preprints (www.preprints.org) | NOT PEER-REVIEWED | Posted: 17 March 2022 doi:10.20944/preprints202203.0251.v1

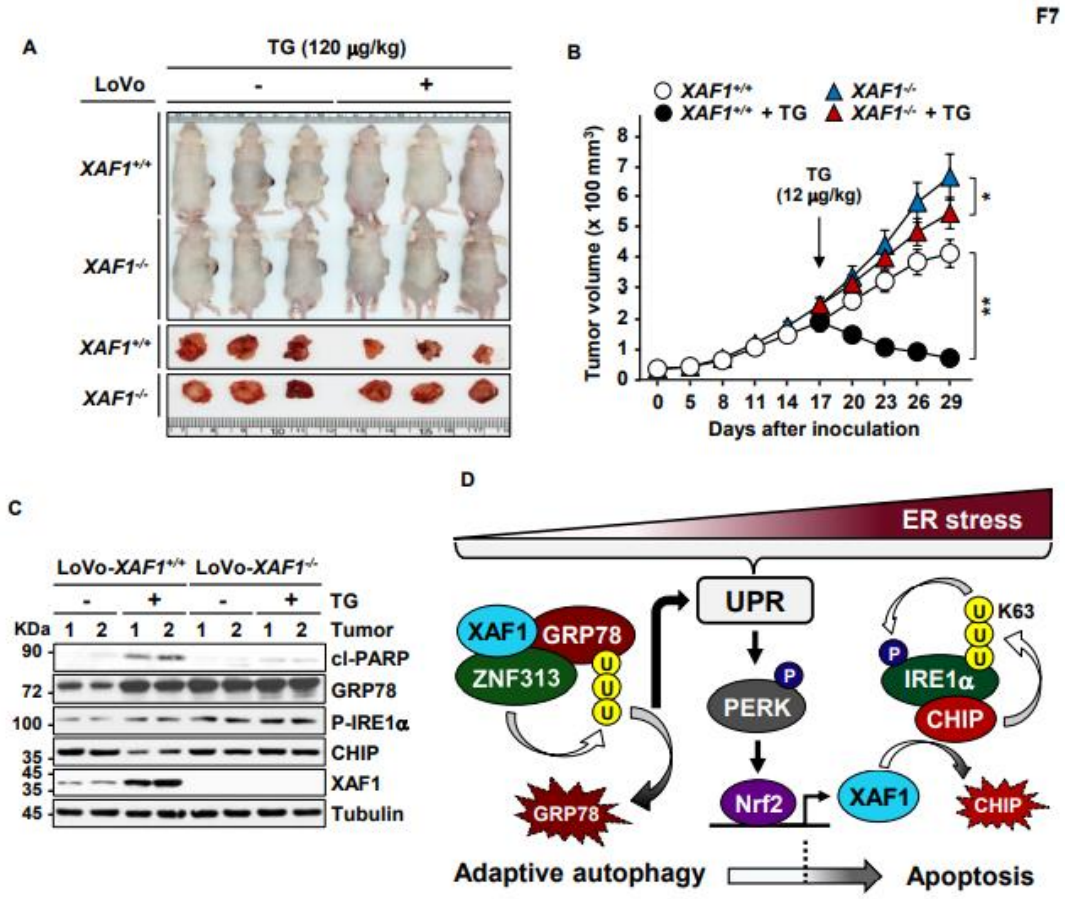

Fig. 7 XAF1 enhances tumor response to cytotoxic ER stress. A, B Mouse tumor xenograft assay showing XAF1 effect on tumor response to TG. Tumors were derived from *XAF1*$^{+/+}$ and *XAF1*$^{-/-}$ sublines of LoVo cells and exposed to saline or TG (12 μg/kg) at day 17 by intratumoral injection. Representative photographs of xenograft tumors at day 29 were shown. Data represent the mean ± SD (n = 6 per group). * $P < 0.05$; ** $P < 0.01$ (Student *t* test). **C** IB assays of GRP78, IRE1α, CHIP in xenograft tumor tissues. **D** Schematic representation of the molecular mechanism underlying XAF1-driven apoptotic switch of ER stress response.

DISCUSSION

Despite accumulating evidence supporting that XAF1 is activated under various stressful conditions and directs an apoptotic switch of a stress response, its role in ER stress response has not been studied yet. In the present study, we identified that XAF1 increases apoptotic sensitivity to ER stress and dictates the outcomes of UPR signaling through the modulation of the ER stress sensor GRP78 and the UPR signal transducer IRE1α. Therefore, our study demonstrates that XAF1 functions as a linchpin to govern the cell-fate decisions under ER stress conditions favoring

Preprints (www.preprints.org) | NOT PEER-REVIEWED | Posted: 17 March 2022 doi:10.20944/preprints202203.0251.v1

apoptosis over adaptation.

GRP78 is the most abundant and major chaperone in the ER, which acts as an ER stress sensor that detects ER imbalance and fine-tunes the threshold for UPR initiation [5, 31]. GRP78 upregulation in multiple human tumors contributes to tumor cell survival and chemoresistance through high tolerance for ER stress while its suppression leads to enhanced cytotoxic response to chemotherapeutic drugs [13-16, 38]. Increased GRP78 expression is associated with higher pathological grades, high risk of recurrence, and poor prognosis of cancer patients [38-42]. Therefore, GRP78 has been suggested as a target for therapeutic intervention. Studies demonstrated that GRP78 is destabilized by various tumor suppressors while it is stabilized by oncogenic factors [43-47]. Nevertheless, the molecular mechanisms underlying GRP78 upregulation in the tumorigenic process have not been well understood. In the current study, we present evidence that XAF1 directly interacts with and destabilizes GRP78 to enhance apoptotic cellular response to ER stress. We also observed an inverse correlation of GRP78 and XAF1 expression in human cancer cell lines of various origins and primary breast carcinoma tissues. Given that loss or reduction of *XAF1* expression by aberrant promoter hypermethylation is common in human cancers, our data support that epigenetic silencing of *XAF1* is a mechanism leading to abnormal elevation of GRP78 and tumor resistance to ER stress.

Upon GRP78 dissociation, UPR signaling transducers IRE1 and PERK are activated through dimerization and autophosphorylation [3]. IRE1 splices *XBP1* mRNA to generate XBP1s, which improves stress adaptation by transactivating genes involved in the ER protein quality control. PERK inhibits global protein synthesis through phosphorylation of eIF2α to reduce ER protein loading. Under prolonged or irreversible ER stress conditions, PERK activity is sustained, while IRE1 phosphorylation is turned off [35, 36]. Attenuated IRE1 signaling dissolves its oligomers and reduces RNase activity, which eventually makes cells sensitive to death [48]. The Nrf2 transcription factor, one of phosphorylation substrates of PERK, activates multiple target genes that are involved

Preprints (www.preprints.org) | NOT PEER-REVIEWED | Posted: 17 March 2022 doi:10.20944/preprints202203.0251.v1

mainly in cytoprotective response to stress [49, 50]. Nrf2 activation increases expression of proteasome-related genes and anti-apoptotic proteins, such as Bcl-2 and Bcl-xL to enhance cell survival and drug resistance [51-53]. Intriguingly, we identified *XAF1* as a *bona fide* transcription target of Nrf2 under ER stress conditions. It is thus plausible that Nrf2 might be modified differentially by cytostatic and cytotoxic stresses, allowing its selective or preferential binding to a subset of target promoters and thereby provoking both adaptive and apoptotic effects depending on its target selectivity. Given that tumor cells with *XAF1* hypermethylation require high dose of stress inducers for XAF1 activation, promoter methylation status of *XAF1* could be a predictive marker for the clinical efficacy of ER stress-based therapy. This is supported by the finding that blockade of XAF1 induction disrupts tumor regression by treatment of ER stress inducer *in vivo*. Considering that Nrf2 and XAF1 are up- and down-regulated, respectively in many human cancers, alteration of the Nrf2-XAF1 axes might contribute to tumor resistance to ER stress. Together, our study establishes XAF1 as a key target of UPR in signaling apoptosis, suggesting that its alteration might be a critical event in the enhanced adaptation function of UPR signaling and the appearance of ER stress resistance in tumorigenesis.

Regulation of IRE1 activity is essential for the cell-fate decisions under ER stress conditions. IRE1 is initially phosphorylated via K63 ubiquitination by CHIP and dephosphorylated during the terminal phase of UPR by RPAP2 phosphatase [37, 54]. However, the molecular mechanism of IRE1 regulation has been poorly understood. Our study shows that XAF1 destabilizes CHIP to suppress K63 ubiquitination and subsequent phosphorylation of IRE1α. Although further studies are required for the molecular understanding of XAF1 regulation of the CHIP-IRE1 axis, our data strongly support that XAF1 induces the proteasomal degradation of CHIP through the assembly of an E3 ligase-mediated destruction complex. Considering that K63 ubiquitination serves as a scaffold for protein-protein interaction and regulates cellular localization of proteins, it is conceivable that XAF1 affects IRE1α binding to proteins and its ER membrane localization [55].

Preprints (www.preprints.org) | NOT PEER-REVIEWED | Posted: 17 March 2022 doi:10.20944/preprints202203.0251.v1

It is thus conceivable that XAF1 blocks stress adaptation function of IRE1α to drive ER stress-mediated apoptosis.

Conclusions

XAF1 represents one crucial molecular switch in ER stress-induced UPR-mediated cell-fate decisions, adding a new layer of complexity to the mechanisms by which the outcomes of UPR signaling is determined. Our study uncovers a novel tumor suppressive role of XAF1, raising the possibility that the restoration of the XAF1-GRP78 and/or XAF1-CHIP-IRE1α interplay could be an attractive avenue for the therapeutic intervention of tumor progression.

MATERIALS AND METHODS

Human cell lines and reagents

Twenty human cancer cell lines derived from colon (RKO, LoVo, DLD-1, HCT116, SW620, SNU-C2A, SNU-C5, and LS174T), bladder (253J, T24, J82, and HT1376), and breast (HCC1937, MDA-MB231, BT-20, T47D, and Hs578T), and brain (A1207, LN18, and LN229) were purchased from the American Type Culture Collection (Rockville, MD, USA) or Korea Cell Line Bank (Seoul, Korea). Cell lines were maintained at 37°C in a 5% CO2 incubator and cultured in RPMI1640, McCoy, or DMEM medium supplemented with 10% fetal bovine serum (FBS) (GenDEPOT, Barker, TX, USA). Human haploid cell line HAP1 and its ZNF313 knockout subline were obtained from Horizon Discovery Ltd (Cambridge, UK). Cyclohexamide (CHX), Thapsigargin (TG), Tunicamycin (TM), Brefeldin A (BFA), GSK2606414, 4μ8C, AEBSF, 3-MA, and Leupeptin were purchased from Sigma Aldrich (Saint Louis, MO, USA). BafA1 was purchased from Millipore Sigma. MG132 (HY-13259) was purchased from AG Scientific Inc (CA, USA).

XAF1-inducible and knockout cell lines

Preprints (www.preprints.org) | NOT PEER-REVIEWED | Posted: 17 March 2022 doi:10.20944/preprints202203.0251.v1

Cell lines with tetracycline-inducible XAF1 system (Tet-XAF1) were generated by co-transfection of XAF1 (pcDNA4/TO) and tetracycline repressor vector (TetR) (Genolution Pharmaceuticals, Seoul, Korea) and selection under blasticidin and zeocin. The *XAF1* knockout sublines of J82, HT1376, T47D, and LoVo were generated using the CRISPR/Cas9 system. Cells were co-transfected with 1 μg of XAF1 CRISPR/Cas9 knockout plasmid (sc-402427, SantaCruz Biotechnology, CA, USA) and 2 μg of XAF1 HDR plasmid (sc-402427-HDR, SantaCruz Biotechnology). After 48 h, cells were screened with puromycin for 3 days. After the selection process, cells were seeded in the 96 well plates as single clones. Individual clones were screened for XAF1 expression using immunoblot assay and DNA-PCR. HT1376 *XAF1*$^{-/-}$ sublines with short hairpin (sh) RNA-mediated CHIP knockdown were established by transfection of sh-CHIP constructs (Genolution Pharmaceuticals Inc) and Zeocin (Invitrogen) selection.

Expression plasmids and siRNAs

Expression vectors for XAF1, GRP78, IRE1α, PERK, ATF6, ZNF313, ATF4, and NRF2 were constructed using a PCR-based approach. CHIP-Myc, HA-Ubiquitin-K63, and HA-Ubiquitin-K48 were purchased from Addgene. Xpress-tagged Ubiquitin plasmid was subcloned by inserting ubiquitin fragment of HA-Ub into His-Xpress vector (Invitrogen). Small interfering RNA (siRNA) duplexes against XAF1 (si-XAF1; 5′-GAGCGCCCUGUUGAGUGUAAGUUCUGC-3′), GRP78 (si-GRP78; 5′-GGAGCGCAUUGAUACUAGA-3′), ATF4 (si-ATF4; 5′-CCAGAUCAUUCCUUUAGUUUA-3′), ATF6 (si-ATF6; 5′-GGUUAGAGGCGAGAUUAAA-3′), CHIP (si-CHIP; 5′ -CUAUGAAGGAGGUUAUUGA-3′), IRE1α (si-IRE1α; 5′-GUAAAUUCAGGACCUAUAA-3′), NRF2 (si-NRF2; 5′-GGAUUAUUAUGACUGUUAA-3′), PERK (si-PERK; 5′-CAACCAUUGUGCUAAUAAA-3′), XAF1 (si-XAF1; 5′-GAGCGCCCUGUUGAGUGUAAGUUCUGC-3′), and ZNF313 (siZNF313-1: 5′-GCUGCCGUAAGAAUUUCUU-3′) were synthesized by Genolution Inc (Seoul, Korea). Control

Preprints (www.preprints.org) | NOT PEER-REVIEWED | Posted: 17 March 2022 doi:10.20944/preprints202203.0251.v1

siRNA duplex (AM4635) served as a negative control was purchased from Applied Biosystems (Thermo Fisher Scientific, Waltham, MA, USA). Transfection of siRNAs or expression plasmids was performed using Neon®Transfection System (Thermo Fisher Scientific) or E-fection in vitro Transfection Reagent (Lugen Sci co., Ltd, Bucheon, Korea).

Reporter constructs and luciferase assay

The *XAF1* promoter region was cloned into the pGL4.14 vector (Promega Corporation, Madison, USA). Cells were co-transfected with 200 ng of reporter plasmids and 20 ng of the β-galactosidase expression plasmid. β-galactosidase activity was measured by Mammalian β-Galactosidase Assay Kit (75707, Thermo Fisher Scientific) according to the manufacturer's protocol and used for normalization. After normalization of each extract for protein content, luciferase activity was measured using Steady-Glo® Luciferase Assay System (E2510, Promega Corporation, Madison, USA) and SpectraMax i3x microplate reader (Molecular Devices, CA, USA).

Semi-quantitative reverse transcription-polymerase chain reaction (RT-PCR)

Briefly, 1 μg of total cellular RNA was converted to cDNA by reverse transcription using random hexamer primers and MoMuLV reverse transcriptase (Invitrogen). PCR was initially performed over a range of cycles (20-40 cycles) by using serially diluted cDNA, and 1:4 diluted cDNA (12.5 ng per 50 μl of PCR) undergoing 24–38 cycles was found within the logarithmic phase of amplification with primers used for primers for *XAF1* (sense; 5′-CAGAAGTCCTCGCTGGAGTTTC-3′ and antisense; 5′-TGAAATTCTTTCCCCTTTCC-3′), *GRP78* (sense; 5′-GCTCGACTCGAATTCCAAAG-3′ and antisense; 5′-TTTGTCAGGGGTCTTTCACC-3′), *ATF6* (sense; 5′-TCCGTGACTAAACCTGTCCTAC-3′ and antisense; 5′-TGACAAGCGGATTCTCGATTTTT-3′), *CHIP* (sense; 5′-TCAAGGAGCAGGGCAATCGTCT-3′ and antisense; 5′-GCATCTTCAGGTAGCACAAGGC-

Preprints (www.preprints.org) | NOT PEER-REVIEWED | Posted: 17 March 2022 doi:10.20944/preprints202203.0251.v1

3′), *IRE1α* (sense; 5′-GA GACGTCATTGCACGTGAATT-3′ and antisense; 5′-AGGTCCTGAATTTACGCAGGT-3′), NRF2 (sense; 5′-GAGAGCCCAGTCTTCATTGC-3′ and antisense; 5′-TGCTCAATGTCCTGTTGCAT-3′), *PERK* (sense; 5′-ATC CCCCATGGAACGACCTG-3′ and antisense; 5′-ACCCGCCAGGGACAAAAATG-3′), *NRF2* (sense; 5′-GAGAGCCCAGTCTTCATTGC-3′ and antisense; 5′-TGCTCAATGTCCTGTTGCAT-3′), *XBP1* (sense; 5′-TTACGAGAGAAAACTCATGGCC-3′ and antisense; 5′-GGGTCCAAGTTGTCCAGAATGC-3′), and an endogenous expression standard gene *GAPDH*. PCR products were resolved on 2% (wt/vol) agarose gels and visualized on a GelDoc (BioRad, Hercules, CA, USA). Quantitation was achieved by densitometric scanning of the ethidium bromide-stained gels. Integration and analysis was performed by using Quantity One software program (Bio-Rad).

Chromatin immunoprecipitation (ChIP)

ChIP assay was carried out using a Simple ChIP™ Enzymatic Chromatin IP Kit (#9003, Cell Signaling Technology, Danvers, MA, USA). Briefly, cells were fixed by 1% formaldehyde for 5 min and then sonicated to prepare chromatin suspensions. Immunoprecipitation analysis was carried out with antibodies specific for NRF2 (#12721, Cell Signaling Technology) or normal rabbit IgG (#2729, Cell Signaling Technology). The *XAF1* promoter region comprising the putative NRF2-binding site (ARE) was amplified using primers P3 (sense; 5′-CCAGCTCTGATGTTGAGCGA-3′) and RP1 (antisense; 5′-TTGCTATGGAAAACAGAGGCAGT-3′).

Immunoblot and immunoprecipitation

Antibodies specific for ATF4 (#11815), ATF6 (ab122987), β-tubulin (T-0198), CHIP (#2895), CHOP (#2895), cleaved PARP (#9541), cleaved Caspase-3 (#9665), eIF2α (#5324), Phospho-

Preprints (www.preprints.org) | NOT PEER-REVIEWED | Posted: 17 March 2022 doi:10.20944/preprints202203.0251.v1

eIF2α (#3398), FLAG (sc-1666384), GFP (sc-9996), GRP78/BiP (ab21685, #3177, sc-13539), GST (sc-33613), HA (Y-11; sc-805), LC3 (#4108), IRE1α (#3294), Phospho-IRE1α (ab48187), PERK (#5683), Phospho-PERK (ab192591), NRF2 (A-10; sc365949, #12721), Ub (sc-8017), XBP-1s (#12782), XAF1 (sc-398012, sc-374020, #13805) and ZNF313 (sc-101116) were purchased from Santa Cruz Biotechnology (Santa Cruz, CA, USA), Cell Signaling Technology, Abcam (Cambridge, MA, USA), and Sigma Aldrich.

Immunohistochemistry

Immunohistochemistry assay for human breast tissues was performed using tissue array slides (US Biomax, MD, USA) and Vectastain ABC (avidin–biotin–peroxidase) kit (Vector Laboratories). Briefly, slides were incubated with XAF1 or GRP78 antibody overnight at 4°C and visualized using an Axio Scan.Z1 microscopy (Carl Zeiss MicroImaging, Inc). The expression levels of XAF1 and GRP78 were evaluated using Zen software (Zeiss, Oberkochen, Germany). For the immunoreactive score, we established as 1 to 5 point system by multiplying the percentage of positive cells by the intensity of the staining score.

Immunofluorescence and microscopic autophagy assay

Cells were fixed with 4% formaldehyde, permeabilized with 100% methanol, and blocked 0.1% Triton X-100. The cells were incubated with anti-XAF1 (A-11, Santa Cruz) antibody at 4°C overnight. Next, cells were washed and incubated for 1 h at room temperature with Alexa488-conjugated anti-rabbit (1:250, A21206), Alexa594-conjugated anti-mouse (1:250, A21206), or Alexa488-conjugated anti-mouse (1:250, A21202) secondary antibodies (Thermo Fisher Scientific). The fluorescence and DIC images were detected using a confocal laser scanning microscope (LSM-800, Carl Zeiss MicroImaging Inc). For autophagy assay, T47D cells were seeded in 2-well chamber slide (154461, Thermo Fisher Scientific) and co-transfected with

Preprints (www.preprints.org) | NOT PEER-REVIEWED | Posted: 17 March 2022 doi:10.20944/preprints202203.0251.v1

GFP-LC3B and either red fluorescent protein (RFP)-control or RFP-XAF1. The cells were treated with TG (200 nM) for 48 h. 3-MA (5 μM) or BafA1 (100 nM) were added 2 h before TG treatment. The cells were fixed in 4% paraformaldehyde for 10 min and fluorescent images of cells showing punctuated changes of GFP-LC3 were obtained with the confocal microscope (LSM510META, Carl Zeiss AG). A minimum of 150 transfected cells were counted to quantify the puncta signals for each sample.

Protein pull-down and *in vitro* binding assay

For *in vitro* binding assay, GST-fused XAF1 (GST-XAF1) proteins overexpressed by IPTG in BL21 strain were purified using Glutathione Sepharose 4B (GE Healthcare, Little Chalfont, UK). N-terminal His-tagged recombinant human ZNF313 and recombinant human GRP78 (ab79139) were purchased from Abcam. The GST-XAF1, r-GRP78 and r-His-ZNF313 proteins were incubated with binding assay buffer for 6 h. Immunocomplexes were separated by incubation with protein-A/G Sepharose for 1 h and subjected to SDS-PAGE for immunoblot analysis.

Ubiquitination assay

Cells were transfected with HA-K63 Ub, HA-K48 Ub or Xpress-Ub plasmids, and expression vectors. Cells were incubated with MG132 (20 μM) for 6 h and cell extracts were prepared in buffer containing complete protease inhibitor (Roche). The lysates were incubated with GRP78 antibody overnight at 4 °C, and protein complexes were pelleted with protein A-agarose beads (Thermo Fisher Scientific). The beads were then washed three times with washing buffer (1M NaCl, 10 mM Tris-Cl (pH 8), 1 mM EDTA, 1% NP-40), and ubiquitin conjugated proteins were eluted by boiling in 2X protein sample buffer and visualized by immunoblot assay.

Apoptosis assay

Preprints (www.preprints.org) | NOT PEER-REVIEWED | Posted: 17 March 2022 doi:10.20944/preprints202203.0251.v1

For flow cytometry assay, cells (5 x 10^4) were seeded in six-well plate in triplicate and transfected with expression vector or siRNA. For sub-G1 fraction analysis, cells were fixed with 70% ethanol and resuspended in 1 ml of PBS containing 100 mg/ml RNase and 50 mg/ml propidium iodide (Sigma). The assay was performed on a FACS Calibur flow cytometer (BD Bioscience) and the cell profile was analyzed using MultiCycle software (Phoenix Flow Systems).

Animal studies

Six-week-old immunodeficient male nude mice (nu/nu) (Orient Bio Inc., Seongnam, Korea) were maintained in pressurized ventilated cages. Briefly, the identical numbers (1 x 10^6) of LoVo subline cells were injected subcutaneously to three mice per group. Animal studies were repeated twice. Tumor growth was monitored periodically, and volume (V) was calculated by using the modified ellipsoidal formula: $V = 1/2 \times \text{length} \times (\text{width})^2$. At day 17, 3 mice of each group were exposed to saline or TG (12 μg/kg) by intratumoral injection, and tumor volume was measured at the beginning of injection and monitored regularly for 29 days. All studies were performed with the approval of Korea University Institutional Animal Care and Use Committee and Korea Animal Protection Law.

Statistical analysis

All experiments, including RT-PCR, reporter luciferase and flow cytometry assays were repeated three times, and the results were presented as mean values ± standard deviation (SD). Mean and SD values were calculated using Microsoft Excel software. A student's *t*-test (GraphPad Prism8 software, CA, USA) was performed to determine the statistical significance. A *P* value of less than 0.05 was considered significant.

REFERENCES

 doi:10.20944/preprints202203.0251.v1

1. Chen X, Cubillos-Ruiz JR. Endoplasmic reticulum stress signals in the tumour and its microenvironment. Nat Rev Cancer. 2021;21:71-88.

2. Song M, Cubillos-Ruiz JR. Endoplasmic reticulum stress responses in intratumoral immune cells: Implications for cancer immunotherapy. Trends Immunol. 2019;40:128-41.

3. Hetz C, Zhang K, Kaufman RJ. Mechanisms, regulation and functions of the unfolded protein response. Nat Rev Mol Cell Biol. 2020;21:421-38.

4. Wang M, Wey S, Zhang Y, Ye R, Lee AS. Role of the unfolded protein response regulator GRP78/BiP in development, cancer, and neurological disorders. Antioxid Redox Signal. 2009;11:2307-16.

5. Luo B, Lee AS. The critical roles of endoplasmic reticulum chaperones and unfolded protein response in tumorigenesis and anticancer therapies. Oncogene. 2013;32:805-18.

6. Urra H, Dufey E, Avril T, Chevet E, Hetz C. Endoplasmic reticulum stress and the hallmarks of cancer. Trends Cancer. 2016;2:252-62.

7. Sicari D, Delaunay-Moisan A, Combettes L, Chevet E, Igbaria A. A guide to assessing endoplasmic reticulum homeostasis and stress in mammalian systems. FEBS J. 2020;287:27-42.

8. Gardner BM, Pincus D, Gotthardt K, Gallagher CM, Walter P. Endoplasmic reticulum stress sensing in the unfolded protein response. Cold Spring Harb Perspect Biol. 2013;5.

9. Szegezdi E, Logue SE, Gorman AM, Samali A. Mediators of endoplasmic reticulum stress-induced apoptosis. EMBO Rep. 2006;7:880-5.

10. Vitale M, Bakunts A, Orsi A, Lari F, Tadè L, Danieli A et al. Inadequate BiP availability defines endoplasmic reticulum stress. Elife. 2019;8:e41168.

11. Chang Y-W, Tseng C-F, Wang M-Y, Chang W-C, Lee C-C, Chen L-T et al. Deacetylation of HSPA5 by HDAC6 leads to GP78-mediated HSPA5 ubiquitination at K447 and suppresses metastasis of breast cancer. Oncogene. 2016;35:1517-28.

12. Zhang Y, Tseng C-C, Tsai Y-L, Fu X, Schiff R, Lee AS. Cancer cells resistant to therapy promote

cell surface relocalization of GRP78 which complexes with PI3K and enhances PI(3,4,5)P3 production. PLoS One. 2013;8:e80071.

13. Lu G, Luo H, Zhu X. Targeting the GRP78 pathway for cancer therapy. Front Med (Lausanne). 2020;7:351.

14. Lee HK, Xiang C, Cazacu S, Finniss S, Kazimirsky G, Lemke N et al. GRP78 is overexpressed in glioblastomas and regulates glioma cell growth and apoptosis. Neuro Oncol. 2008;10:236-43.

15. Pyrko P, Schonthal AH, Hofman FM, Chen TC, Lee AS. The unfolded protein response regulator GRP78/BiP as a novel target for increasing chemosensitivity in malignant gliomas. Cancer Res. 2007;67:9809-16.

16. He Y, Su J, Lan B, Gao Y, Zhao J. Targeting off-target effects: endoplasmic reticulum stress and autophagy as effective strategies to enhance temozolomide treatment. Onco Targets Ther. 2019;12:1857-65.

17. Liston P, Fong WG, Kelly NL, Toji S, Miyazaki T, Conte D et al. Identification of XAF1 as an antagonist of XIAP anti-Caspase activity. Nat Cell Biol. 2001;3:128-33.

18. Fong WG, Liston P, Rajcan-Separovic E, St. Jean M, Craig C, Korneluk RG. Expression and genetic analysis of XIAP-associated factor 1 (XAF1) in cancer cell lines. Genomics. 2000;70:113-22.

19. Byun D-S, Cho K, Ryu B-K, Lee M-G, Kang M-J, Kim H-R et al. Hypermethylation of XIAP-associated factor 1, a putative tumor suppressor gene from the 17p13.2 locus, in human gastric adenocarcinomas. Cancer Res. 2003;63:7068-75.

20. Chung SK, Lee MG, Ryu BK, Lee JH, Han J, Byun DS et al. Frequent alteration of XAF1 in human colorectal cancers: Implication for tumor cell resistance to apoptotic stresses. Gastroenterology. 2007;132:2459-77.

21. Lee M-G, Huh J-S, Chung S-K, Lee J-H, Byun D-S, Ryu B-K et al. Promoter CpG hypermethylation and downregulation of XAF1 expression in human urogenital malignancies:

 doi:10.20944/preprints202203.0251.v1

implication for attenuated p53 response to apoptotic stresses. Oncogene. 2006;25:5807-22.

22. Han J, Kim YL, Lee KW, Her NG, Ha TK, Yoon S, et al. ZNF313 is a novel cell cycle activator with an E3 ligase activity inhibiting cellular senescence by destabilizing p21(WAF1). Cell Death Differ. 2013;20:1055-67.

23. Lee M-G, Han J, Jeong S-I, Her N-G, Lee J-H, Ha T-K et al. XAF1 directs apoptotic switch of p53 signaling through activation of HIPK2 and ZNF313. Proc Natl Acad Sci USA. 2014;111:15532-37.

24. Xia Y, Novak R, Lewis J, Duckett CS, Phillips AC. Xaf1 can cooperate with TNF alpha in the induction of apoptosis, independently of interaction with XIAP. Mol Cell Biochem. 2006;286:67-76.

25. Leaman DW, Chawla-Sarkar M, Vyas K, Reheman M, Tamai K, Toji S et al. Identification of X-linked inhibitor of apoptosis-associated factor-1 as an interferon-stimulated gene that augments TRAIL Apo2L-induced apoptosis. J Biol Chem. 2002;277:28504-11.

26. Micali OC, Cheung HH, Plenchette S, Hurley SL, Liston P, LaCasse EC et al. Silencing of the XAF1 gene by promoter hypermethylation in cancer cells and reactivation to TRAIL-sensitization by IFN-beta. BMC Cancer. 2007;7:52.

27. Zhu LM, Shi DM, Dai Q, Cheng XJ, Yao WY, Sun PH et al. Tumor suppressor XAF1 induces apoptosis, inhibits angiogenesis and inhibits tumor growth in hepatocellular carcinoma. Oncotarget. 2014;5:5403-15.

28. Wang J, Gu Q, Li M, Zhang W, Yang M, Zou B et al. Identification of XAF1 as a novel cell cycle regulator through modulating G(2)/M checkpoint and interaction with checkpoint kinase 1 in gastrointestinal cancer. Carcinogenesis. 2009;30:1507-16.

29. Jeong S-I, Kim J-W, Ko K-P, Ryu B-K, Lee M-G, Kim H-J et al. XAF1 forms a positive feedback loop with IRF-1 to drive apoptotic stress response and suppress tumorigenesis. Cell Death Dis. 2018;9:806.

 doi:10.20944/preprints202203.0251.v1

30. Shin C-H, Lee M-G, Han J, Jeong S-I, Ryu B-K, Chi S-G. Identification of XAF1–MT2A mutual antagonism as a molecular switch in cell-fate decisions under stressful conditions. Proc Natl Acad Sci USA. 2017;114:5683-8.

31. Lee AS. The glucose-regulated proteins: stress induction and clinical applications. Trends Biochem Sci. 2001;26:504-10.

32. Liu Z, Lv Y, Zhao N, Guan G, Wang J. Protein kinase R-like ER kinase and its role in endoplasmic reticulum stress-decided cell fate. Cell Death Dis. 2015;6:e1822.

33. Denton D, Kumar S. Autophagy-dependent cell death. Cell Death Differ. 2019;26:605-16.

34. Arora V, Cheung HH, Plenchette S, Micali OC, Liston P, Korneluk RG. Degradation of survivin by the X-linked inhibitor of apoptosis (XIAP)-XAF1 complex. J Biol Chem. 2007;282:26202-9.

35. Lin JH, Li H, Yasumura D, Cohen HR, Zhang C, Panning B et al. IRE1 signaling affects cell fate during the unfolded protein response. Science. 2007;318:944-9.

36. Lin JH, Li H, Zhang Y, Ron D, Walter P. Divergent effects of PERK and IRE1 signaling on cell viability. PLoS One. 2009;4:e4170.

37. Zhu X, Zhang J, Sun H, Jiang C, Dong Y, Shan Q et al. Ubiquitination of inositol-requiring enzyme 1 (IRE1) by the E3 ligase CHIP mediates the IRE1/TRAF2/JNK pathway. J Biol Chem. 2014;289:30567-77.

38. Lee E, Nichols P, Spicer D, Groshen S, Yu MC, Lee AS. GRP78 as a novel predictor of responsiveness to chemotherapy in breast cancer. Cancer Res. 2006;66:7849-53.

39. Kang JM, Park S, Kim SJ, Kim H, Lee B, Kim J et al. KIAA1324 suppresses gastric cancer progression by inhibiting the oncoprotein GRP78. Cancer Res. 2015;75:3087-97.

40. Kaira K, Toyoda M, Shimizu A, Imai H, Sakakura K, Nikkuni O et al. Decreasing expression of glucose-regulated protein GRP78/BiP as a significant prognostic predictor in patients with advanced laryngeal squamous cell carcinoma. Head Neck. 2016;38:1539-44.

41. Qian Y, Wong CC, Xu J, Chen H, Zhang Y, Kang W et al. Sodium channel subunit SCNN1B

 doi:10.20944/preprints202203.0251.v1

suppresses gastric cancer growth and metastasis via GRP78 degradation. Cancer Res. 2017;77:1968-82.

42. Kim SY, Kim HJ, Kim HJ, Kim DH, Han JH, Byeon HK et al. HSPA5 negatively regulates lysosomal activity through ubiquitination of MUL1 in head and neck cancer. Autophagy. 2018;14:385-403.

43. Kang JM, Park S, Kim SJ, Kim H, Lee B, Kim J et al. KIAA1324 suppresses gastric cancer progression by inhibiting the oncoprotein GRP78. Cancer Res. 2015;75:3087-97.

44. Qian Y, Wong CC, Xu J, Chen H, Zhang Y, Kang W et al. Sodium channel subunit SCNN1B suppresses gastric cancer growth and metastasis via GRP78 degradation, Cancer Res. 2017;77:1968-82.

45. Wang X, Wu X, Wang Q, Zhang Y, Wang C, Chen J. NLRP6 suppresses gastric cancer growth via GRP78 ubiquitination. Exp Cell Res. 2020;395:112177.

46. Chen L, Xu S, Liu L, Wen X, Xu Y, Chen J et al. Cab45S inhibits the ER stress-induced IRE1-JNK pathway and apoptosis via GRP78/BiP. Cell Death Dis. 2014;5;e1219.

47. Du T, Li H, Fan Y, Yuan L, Guo X, Zhu Q et al. The deubiquitylase OTUD3 stabilizes GRP78 and promotes lung tumorigenesis, Nat Commun. 2019;10:2914.

48. Siwecka N, Rozpedek-Kaminska W, Wawrzynkiewicz A, Pytel D, Diehl JA, Majsterek I. The structure, activation and signaling of IRE1 and its role in determining cell fate. Biomedicines. 2021;9:156.

49. Cullinan SB, Zhang D, Hannink M, Arvisais E, Kaufman RJ, Diehl JA. Nrf2 is a direct PERK substrate and effector of PERK-dependent cell survival. Mol Cell Biol. 2003;23:7198-209.

50. Cullinan SB, Diehl JA. Coordination of ER and oxidative stress signaling: the PERK/Nrf2 signaling pathway. Int J Biochem Cell Biol. 2006;38:317-32.

51. Zanotto-Filho A, Masamsetti VP, Loranc E, Tonapi SS, Gorthi A, Bernard X et al. Alkylating agent-induced NRF2 blocks endoplasmic reticulum stress-mediated apoptosis via control of

glutathione pools and protein thiol homeostasis. Mol Cancer Ther. 2016;15:3000-14.

52. Niture SK, Jaiswal AK. Nrf2-induced antiapoptotic Bcl-xL protein enhances cell survival and drug resistance. Free Radic Biol Med. 2013;57:119-31.

53. Niture SK, Jaiswal AK. Nrf2 protein up-regulates antiapoptotic protein Bcl-2 and prevents cellular apoptosis. J Biol Chem. 2012;287:9873-86.

54. Chang TK, Lawrence DA, Lu M, Tan J, Harnoss JM, Marsters SA et al. Coordination between two branches of the unfolded protein response determines apoptotic cell fate. Mol Cell. 2018;71:629-36.

55. Wang G, Gao Y, Li L, Jin G, Cai Z, Chao JI et al. K63-linked ubiquitination in kinase activation and cancer. Front Oncol. 2012;2:5.

ACKNOWLEDGEMENTS

This work was supported in part by National Research Foundation of Korea (Grant numbers NRF-2021R1A2B03002487, S.-G.C. and NRF-2018R1D1A1B07041512, M.-G.L.), and National Cancer Center of Korea (HA17C0034, S.-G.C.).

AUTHOR CONTRIBUTIONS

K-WL, H-RH, J-SL, and K-PK performed experiments. M-GL, and S-GC provided interpretation of the data. K-WL and S-GC wrote the manuscript. S-GC is responsible for the designing and funding collections. All authors have approved this manuscript.

COMPETING INTERSESTS

The authors declare that they have no conflict of interest.

Preprints (www.preprints.org) | NOT PEER-REVIEWED | Posted: 17 March 2022 doi:10.20944/preprints202203.0251.v1

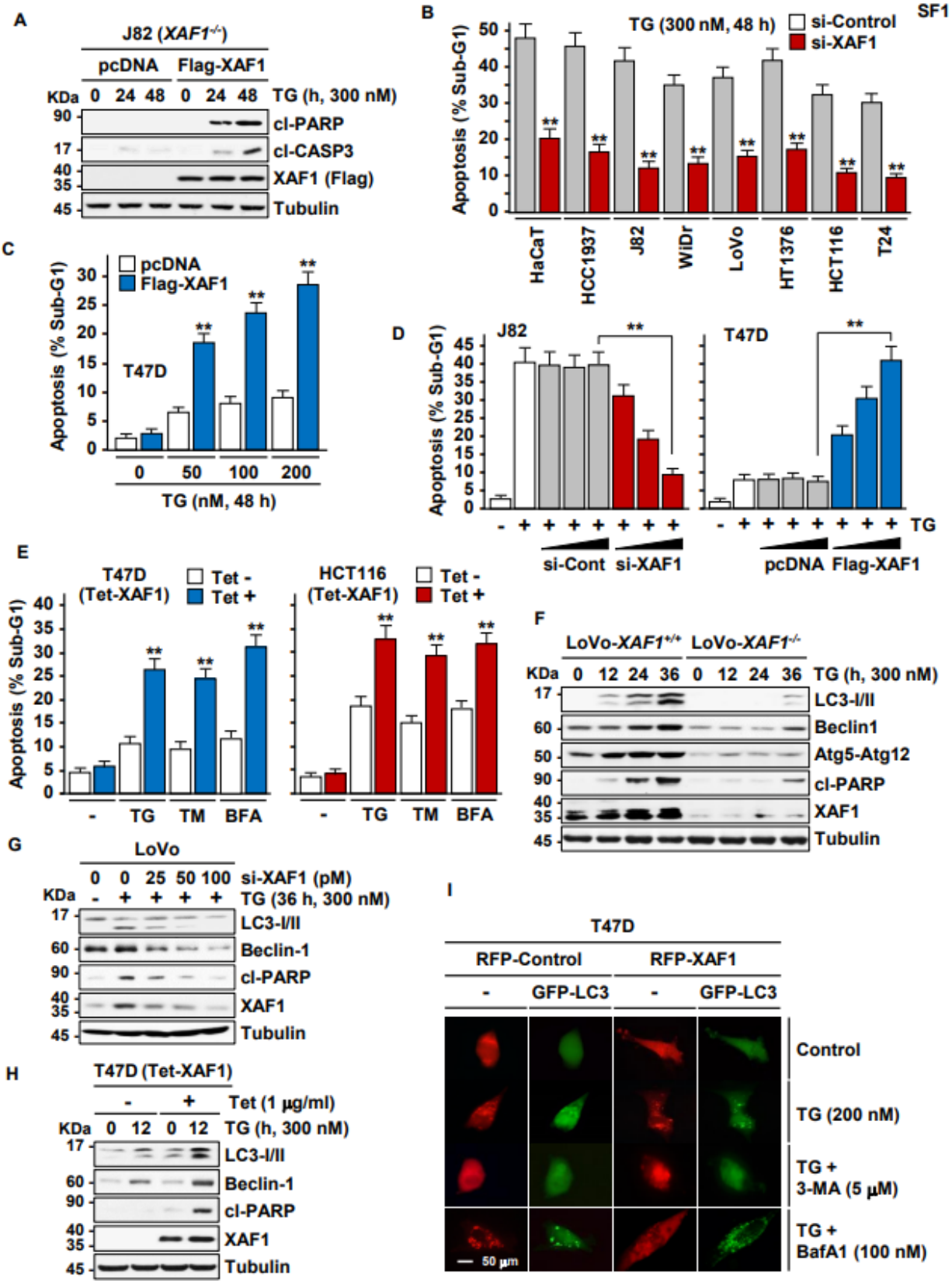

Preprints (www.preprints.org) | NOT PEER-REVIEWED | Posted: 17 March 2022 doi:10.20944/preprints202203.0251.v1

Fig. S1 A Recovery of apoptotic sensitivity of J82-*XAF1*$^{-/-}$ subline cells by ectopic expression of XAF1. Cells were transfected with 2 μg of pcDNA (control) or Flag-XAF1 plasmids. IB assay of cleaved PARP and cl-CASP3 levels was carried out to detect TG-induced apoptosis. **B** Effect of XAF1 knockdown on TG-induced apoptosis in human cancer cell lines. Cells were transfected with 50 pM of si-Control or si-XAF1 and then exposed to TG. Apoptosis induction was determined by flow cytometric analysis of sub-G1 fraction. **C** Apoptosis-promoting effect of XAF1. T47D cells were transfected with pcDNA (control) or Flag-XAF1 plasmids and then exposed to an increasing dose of TG as indicated. Apoptosis induction was measured by flow cytometric analysis of sub-G1 fraction. **D** Effect of XAF1 depletion and expression on TG-induced apoptosis. Cells were transfected with an increasing dose of si-XAF1 or Flag-XAF1 and then exposed to TG (300 nM, 48 h). **E** Effect of XAF1 induction on apoptotic sensitivity to ER stress inducers. XAF1 induction was achieved by Tet-inducible XAF1 (Tet-XAF1) system. Cells were treated with TG (300 nM), TM (1 μg/ml), or BFA (2 μg/ml) for 48 h. **F** Autophagy-promoting effect of XAF1. *XAF1*$^{+/+}$ and *XAF1*$^{-/-}$ sublines of LoVo were treated with TG as indicated. LC3-I/II, Beclin-1, and Atg5-Atg12 were used as markers of autophagy induction. **G** Effect of XAF1 depletion on TG-induced autophagy and apoptosis in LoVo cells. **H** Effect of XAF1 induction on TG-induced autophagy and apoptosis in T47D cells. XAF1 induction was achieved by Tet-inducible XAF1 (Tet-XAF1) system. **I** Immunofluorescence microscopic analysis of LC3B puncta showing autophagy-stimulating function of XAF1. GFP-LC3 and RFP-XAF1 were transfected to detect LC3B puncta and XAF1 expression, respectively. Cells were exposed to 3-MA or BafA1 at 2 h before TG treatment (200 nM, 36 h). Data represent the mean ± SD of triplicate assays. * $P < 0.05$; ** $P < 0.01$ (Student *t* test).

Preprints (www.preprints.org) | NOT PEER-REVIEWED | Posted: 17 March 2022 doi:10.20944/preprints202203.0251.v1

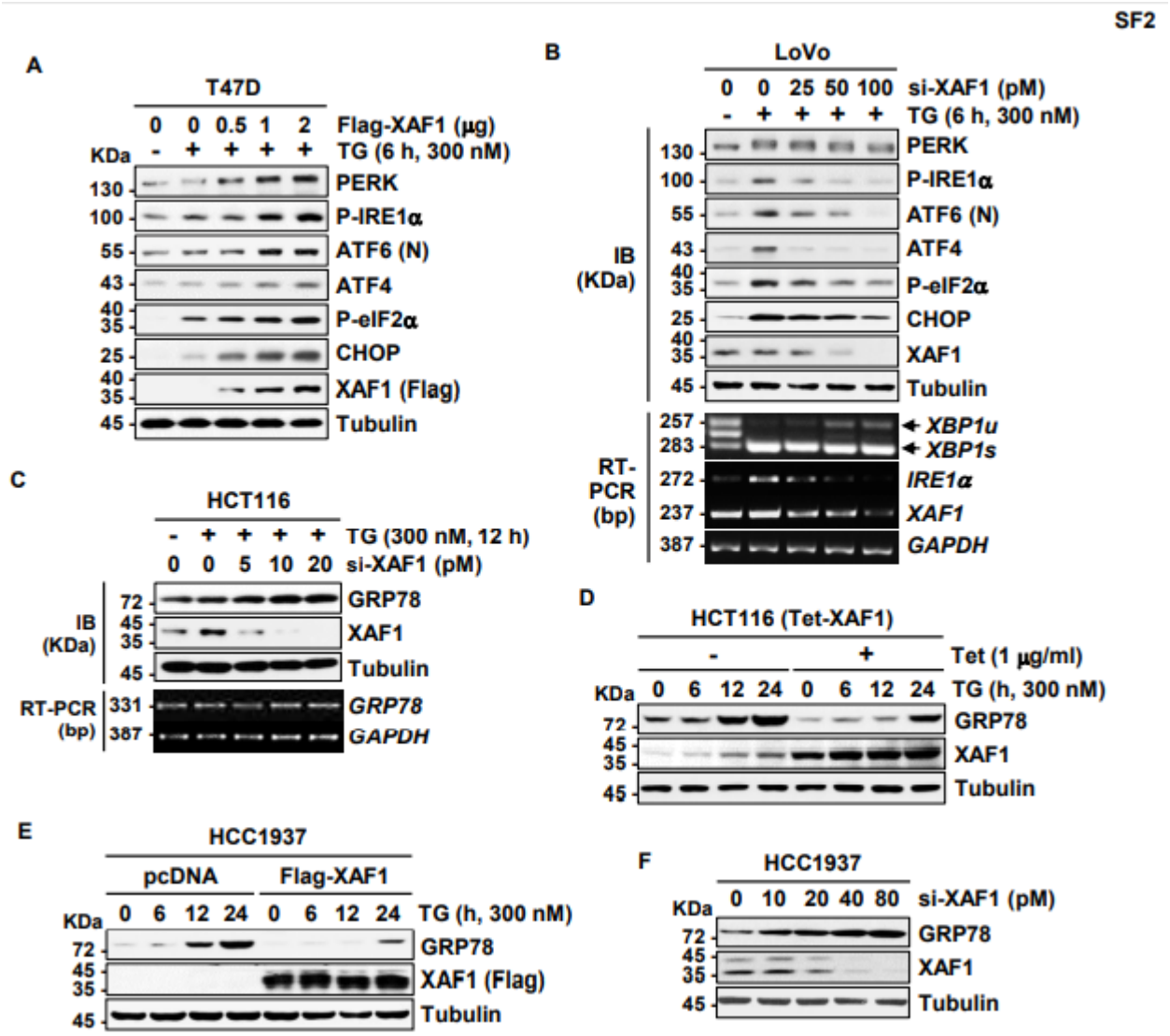

Fig. S2 A XAF1 activation of TG-induced UPR signaling. Cells were transfected with an increasing dose of Flag-XAF1. The cells were treated with TG for 6 h. **B** Effect of XAF1 knockdown on TG activation of UPR signaling in LoVo cells. **C** Upregulation of GRP78 protein level by XAF1 depletion. Cells were transfected with an increasing dose of si-XAF1 as indicated and then treated with TG (300 nM) for 12 h. IB assay was carried out at 48 h after transfection. **D** Effect of XAF1 expression on GRP78 expression. XAF1 induction was achieved using the Tet-XAF1 system and the cells were treated with TG (300 nM) as indicated. **E** Effect of XAF1 overexpression on GRP78 level in TG-treated HCC1937 cells. **F** Effect of XAF1 depletion on GRP78 level in HCC1937 cells.

Preprints (www.preprints.org) | NOT PEER-REVIEWED | Posted: 17 March 2022 doi:10.20944/preprints202203.0251.v1

SF3

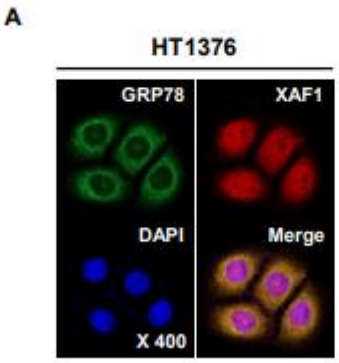

Fig. S3 Immunofluorescence microscopic analysis of cellular localization of GRP78 and XAF1 in HT1376 cells. DAPI was used for counterstaining of the nuclei.

SF4

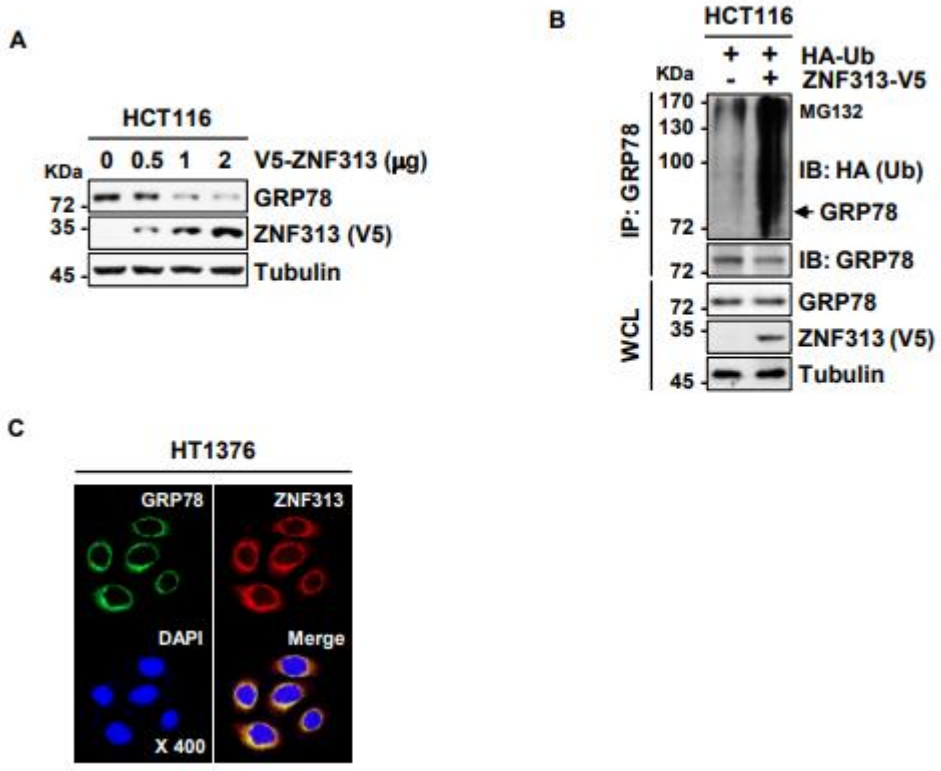

Fig. S4 A Reduction of GRP78 protein level by ZNF313 expression. HCT116 cells were transfected with an increasing dose of V5-ZNF313. IB assay was carried out at 48 h after transfection. **B** IP assay showing ZNF313 induction of GRP78 ubiquitination. **C** Immunofluorescence microscopic analysis of cellular localization of GRP78 and ZNF313 in HT1376 cells. DAPI was used for counterstaining of the nuclei.

Preprints (www.preprints.org) | NOT PEER-REVIEWED | Posted: 17 March 2022 doi:10.20944/preprints202203.0251.v1

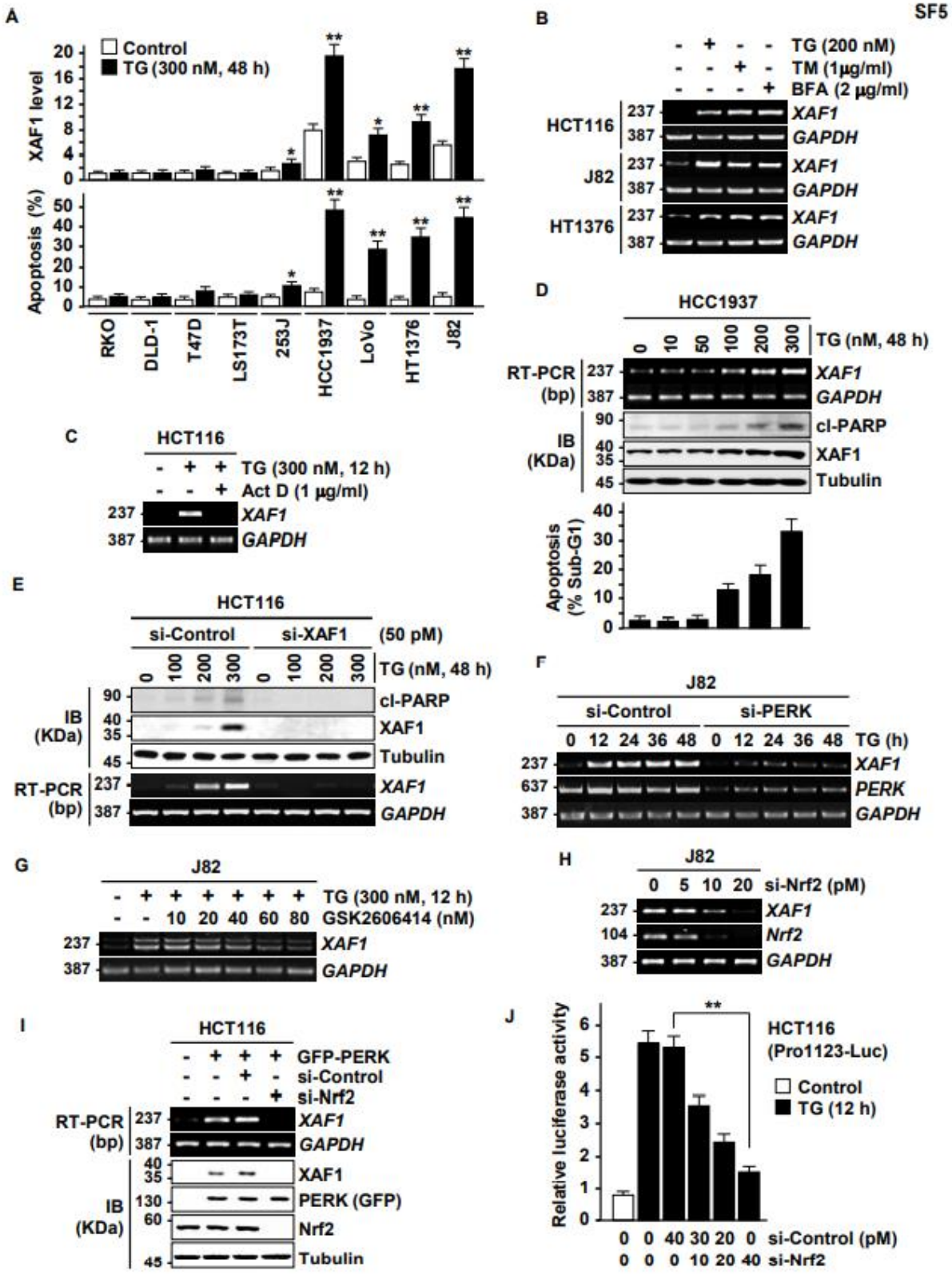

Preprints (www.preprints.org) | NOT PEER-REVIEWED | Posted: 17 March 2022 doi:10.20944/preprints202203.0251.v1

Fig. S5 A XAF1 induction by TG and its association with apoptosis induction in human cell lines. **B** Induction of *XAF1* mRNA in response to ER stress inducers. Cells were treated with TG, TM, and BFA for 12 h. **C** Blockade of TG induction of *XAF1* mRNA by actinomycin D (Act D). Cells were pretreated with Act D for 2 h before TG exposure. **D** Activation of *XAF1* mRNA expression by cytotoxic doses of TG in HCC1937 cells. **E** Loss of cytotoxic TG effect by blockade of XAF1 induction. **F, G** Disruption of TG induction of *XAF1* by depletion of PERK or pretreatment of GSK2606414.**H** Disruption of TG induction of *XAF1* by Nrf2 depletion. **I** XAF1 induction by ectopic expression of PERK and its attenuation by Nrf2 depletion. **J** TG activation of the reporter containing the putative ARE (Pro1123-Luc) and its attenuation by Nrf2 depletion. Cells were transfected with the reporter and then exposed to TG (300 nM) for 12 h.

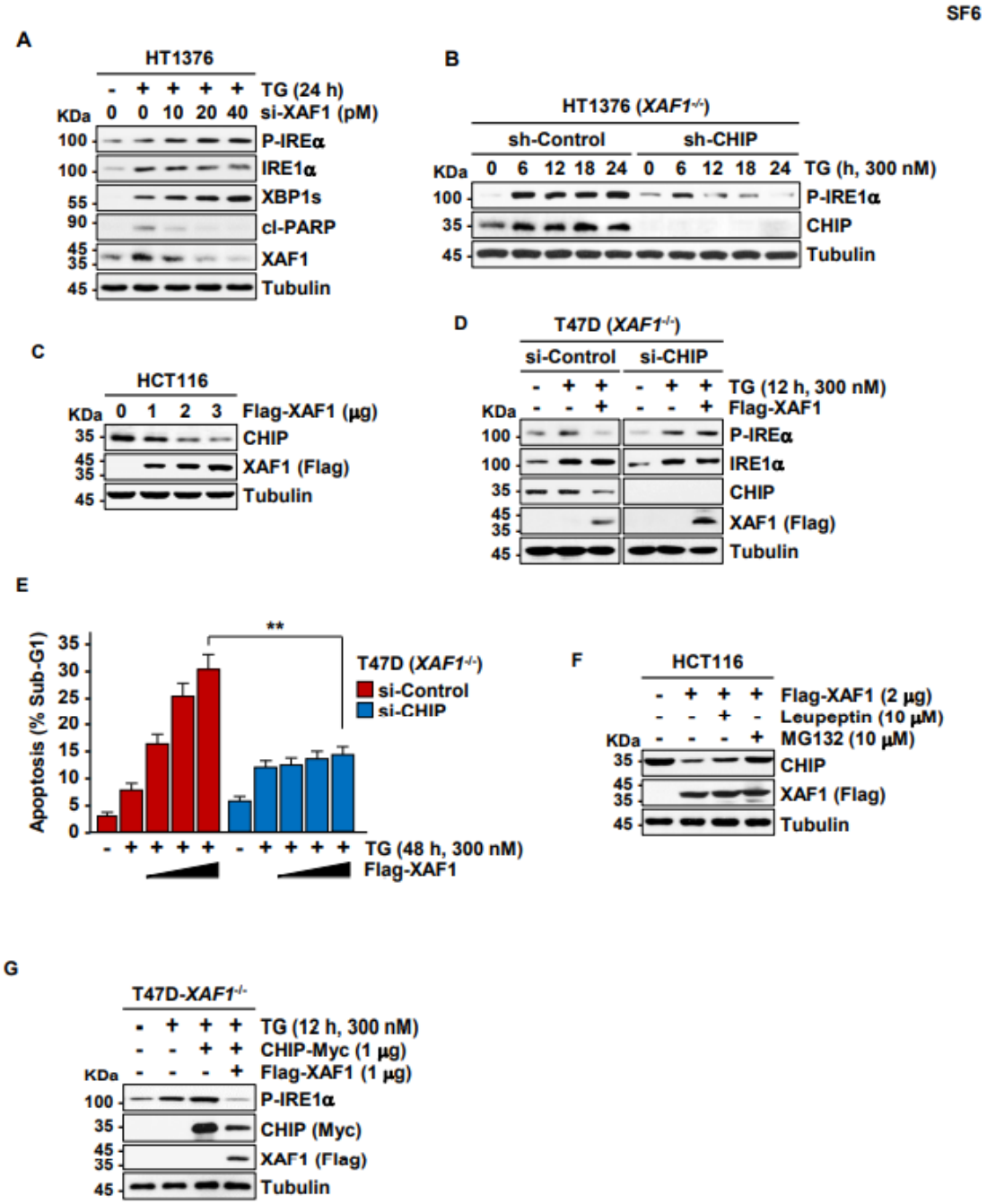

Preprints (www.preprints.org) | NOT PEER-REVIEWED | Posted: 17 March 2022 doi:10.20944/preprints202203.0251.v1

Fig. S6 A Effect of XAF1 depletion on TG-induced IRE1α phosphorylation and XBP1s expression. HT1376 cells were transfected with an increasing dose of si-XAF1 and then treated with TG (300 nM) for 24 h. **B** Effect of CHIP knockdown on TG-induced IRE1α phosphorylation. Expression levels of phosphorylated IRE1α were compared in sh-Control and sh-CHIP sublines of HT1376-*XAF1*$^{-/-}$ cells. **C** Effect of ectopic overexpression of XAF1 on phosphorylated IREα level. HCT116 cells were transfected with an increasing dose of Flag-XAF1. IB was carried out at 48 h after transfection. **D, E** A CHIP dependency of XAF1 effect on TG-induced IREα phosphorylation and apoptosis. T47D-*XAF1*$^{-/-}$ cells were treated with 50 pM of si-Control or si-CHIP and then exposed to TG (300 nM) for 12 h. **F** Blockade of XAF1-induced CHIP reduction by MG132. HCT116 cells transfected with Flag-XAF1 were exposed to MG132 (10 μM) or Leupeptin (10 μM) for 6 h before harvest. **G** XAF1 suppression of CHIP-mediated IRE1α phosphorylation.